GEM/CEDAR 2016

Aurora and ionosphere/thermosphere coupling

Marc Lessard
University of New Hampshire

Contributions from H. Kim, M. Zettergen, S. Jones , K. Oksavik and many, many others...

Relevant types of aurora

Substorm expansion phase:

1. Inverted-V arcs: 5-20 keV isotropic electrons; arcs with north-south extent of ~10 km, very long east-west extent.
2. Alfvenic arcs: 100-200 eV field-aligned electrons; tall, thin arcs at higher altitudes.

Substorm recovery phase:

1. Pulsating aurora: typically, 10s to several 10s of keV electrons; aurora occurs in pulsating patches, maybe 50+ km in extent, with periods of 8-20 seconds. Patches are often only a few km thick, but at lower altitudes (~95 km).

Cusp aurora:

1. Poleward Moving Auroral Forms (PMAF): Similar to Alfvenic aurora, with arcs the order a 1 km “thick”.
2. Traveling Convection Vortices (TCV): Soft electron precipitation, transient event with vortical ionospheric flows. General motion poleward from near the cusp.

Auroral currents and electric fields

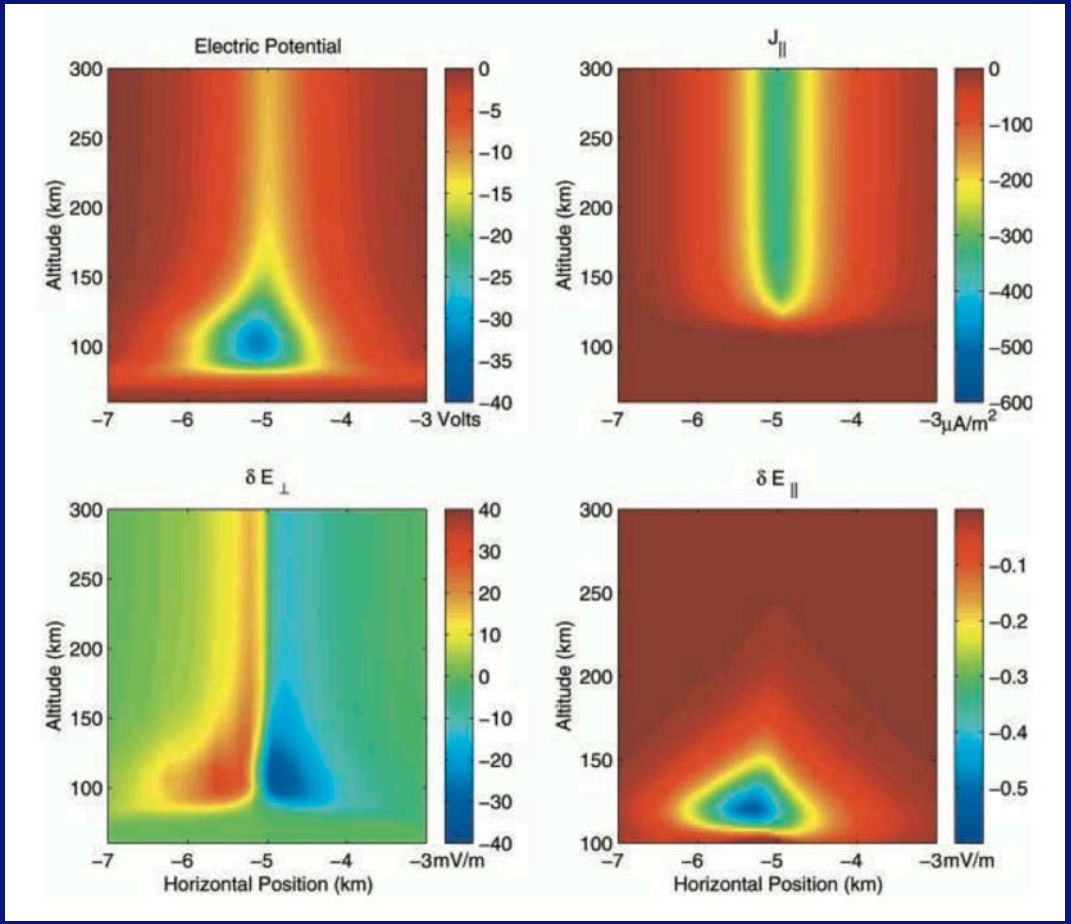

J.-M. A. Noel, J.-P. St.-Maurice, P.-L. Blelly, Nonlinear model of short-scale electrodynamics in the auroral ionosphere, Ann. Geophysicae 18, 1128-1144, 2000.

Auroral currents and electric fields

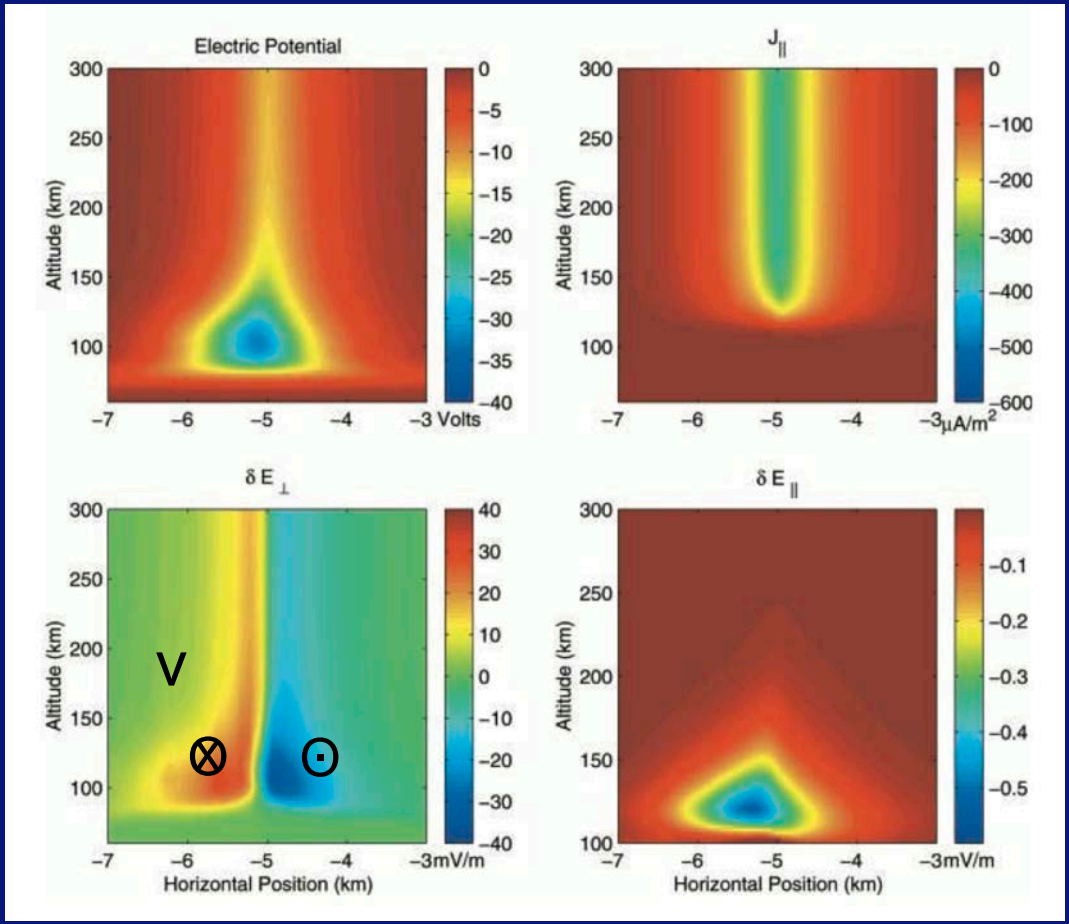

J.-M. A. Noel, J.-P. St.-Maurice, P.-L. Blelly, Nonlinear model of short-scale electrodynamics in the auroral ionosphere, Ann. Geophysicae 18, 1128-1144, 2000.

Historical perspective

First connection to solar activity explained by Luigi Jacchia [Nature, Volume 183, Issue 4660, pp. 526-527, 1959]:

“the orbital acceleration of artificial Earth satellites shows fluctuations which cannot be explained on gravitational ground. It was suggested, rather, that the rotation of the Sun, which has a synodic period of 27 days, could be responsible for changes in upper-atmosphere densities through variable radiation.”

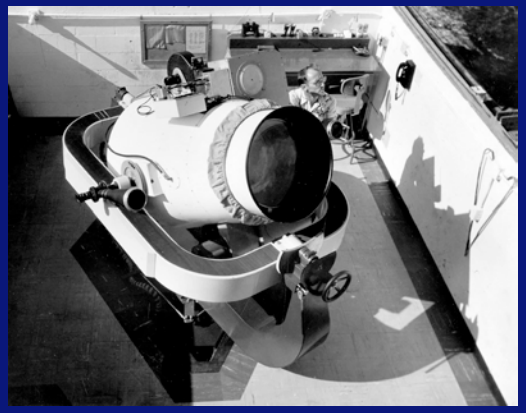

Baker-Nunn camera, used for satellite tracking in late 1950s. Note the person behind the camera, which weighs 3.5 tons! Courtesy of Smithsonian Astrophysical Observatory Archives.

First connection to ionospheric dynamics noted by Jacchia and Slowey [Journal of Geophysical Research, vol. 69, issue 5, pp. 905-910, 1964]

Substorm expansion phases

First connection to aurora reported by L. Devries, NASA TM X-64568, 1971. The Air Force developed an experiment to calibrate an accelerometer to measure satellite drag, known as LOGACS (Low-G Accelerometer Calibration System). Satellite had perigee of 145 km, apogee of 357 km.

Main conclusion is the occurrence of enhanced drag in the vicinity of the auroral electrojet; drag again attributed to Joule heating. Density increase propagated to mid-latitudes after a few hours.

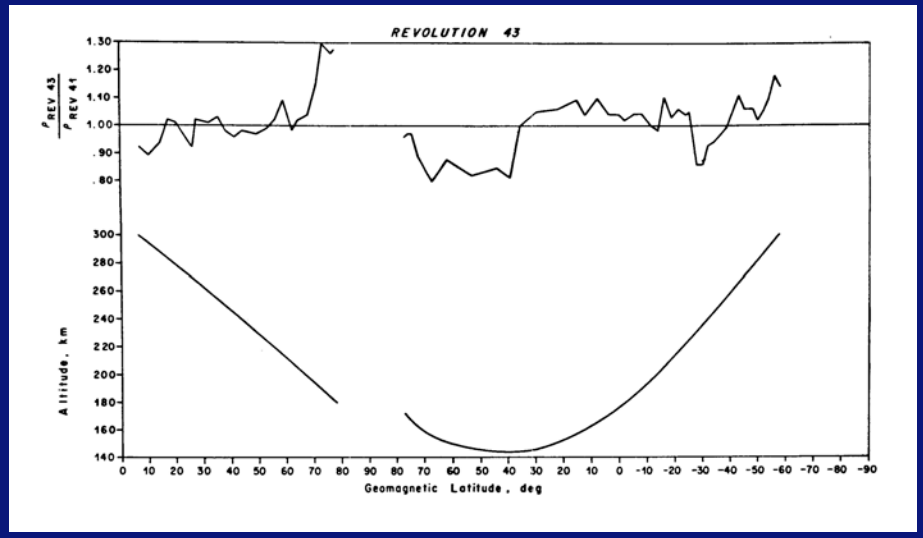

Upper panel shows relative density; lower panel shows spacecraft altitude. This orbit occurred during Ap=56, which increased density to a factor of 1.3.

R. R. Allan, Upper Atmopshere heating near the Auroral Zone, Nature, 235, 1974 extends these results to 400 km altitude, using Molniya orbital data

Substorm expansion phases

At nearly the same time, C. Wilson from UAF used *ground-based* infrasonic microphones to measure waves associated with aurora (C. Wilson and S. Nichparenko, Infrasonic Waves and Auroral Activity, Nature ***214,*** 1299-1302, 1967).

These were named “auroral infrasonic bow waves (AIW) “, and they attribute AIW signatures to the supersonic movement of large scale auroral forms. Mechanism involves **JxB** force and/or Joule heating.

Followed by:
C. Wilson, Auroral Infrasonic Waves, Journal of Geophysical Research, Volume 74, Issue 7, pp. 1812-183, 1969.

“Electrodynamic drift and joule heating associated with the auroral electrojets in auroras that produce infrasonic shock waves are accepted as the basic processes that generate the initial acoustic pulse within a moving auroral form. “

Substorm expansion phases

However....from Wilson, C. R. (1972), Auroral infrasonic wave-generation mechanism, J. Geophys. Res., 77, 1820–1843:

Infrasound waves generated by supersonic auroral arcs are never observed propagating in a poleward direction. Motion is invariably transverse to the auroral.

Even highly supersonic poleward motions of arcs with strong electrojets do not produce infrasonic bow waves.

Me: about electrojet versus current closure in arcs

Substorm expansion phases

V. Pasko (Infrasonic waves generated by supersonic auroral arcs, GRL, *39*, L19105, doi:10.1029/2012GL053587, 2012) followed up on this work...

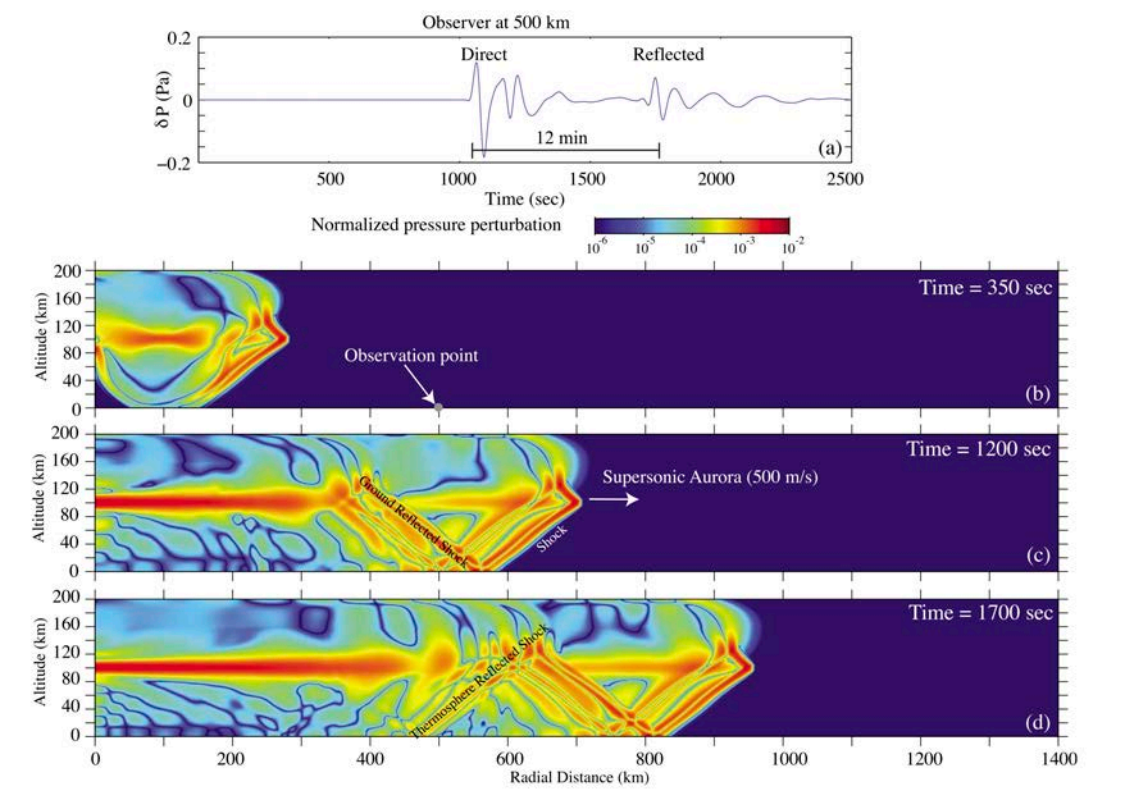

Modeling results: infrasonic waves generated by a supersonic auroral arc moving with velocity 500 m/s. Waves bounce between the ground and the thermosphere.

Gravity waves

Generation of atmospheric gravity waves associated with auroral activity in the polar F region, S. Oyama, M. Ishii, Y. Murayama, H. Shinagawa, S. C. Buchert, R. Fujii and W. Kofman, JGR 106, A9, 18,543-18,554, 2001

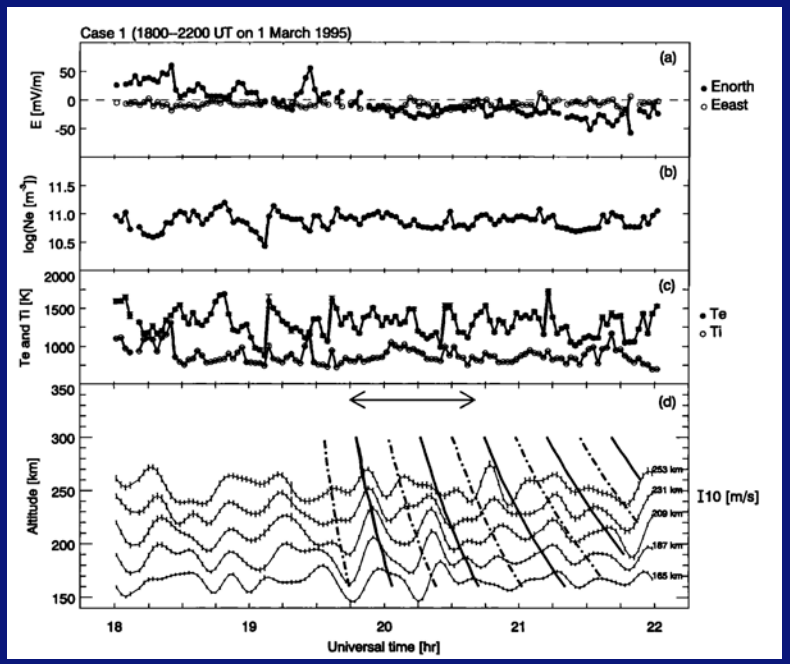

Electric fields derived from EISCAT. Note the peak just after 1900 UT, from an arc.

Electron density at 209 km, from EISCAT

Electron and ion temperatures. The peak in ion temperature near 1900 UT indicates Joule heating.

Vertical neutral winds, observed and modeled.

The point of this paper is to show that gravity waves were driven by Joule heating associated with aurora. Of importance is the fact that the periods are shorter than the natural (Brunt-Vaisala) frequency of these wave (and match the ion heating peaks).

Substorm recovery phases

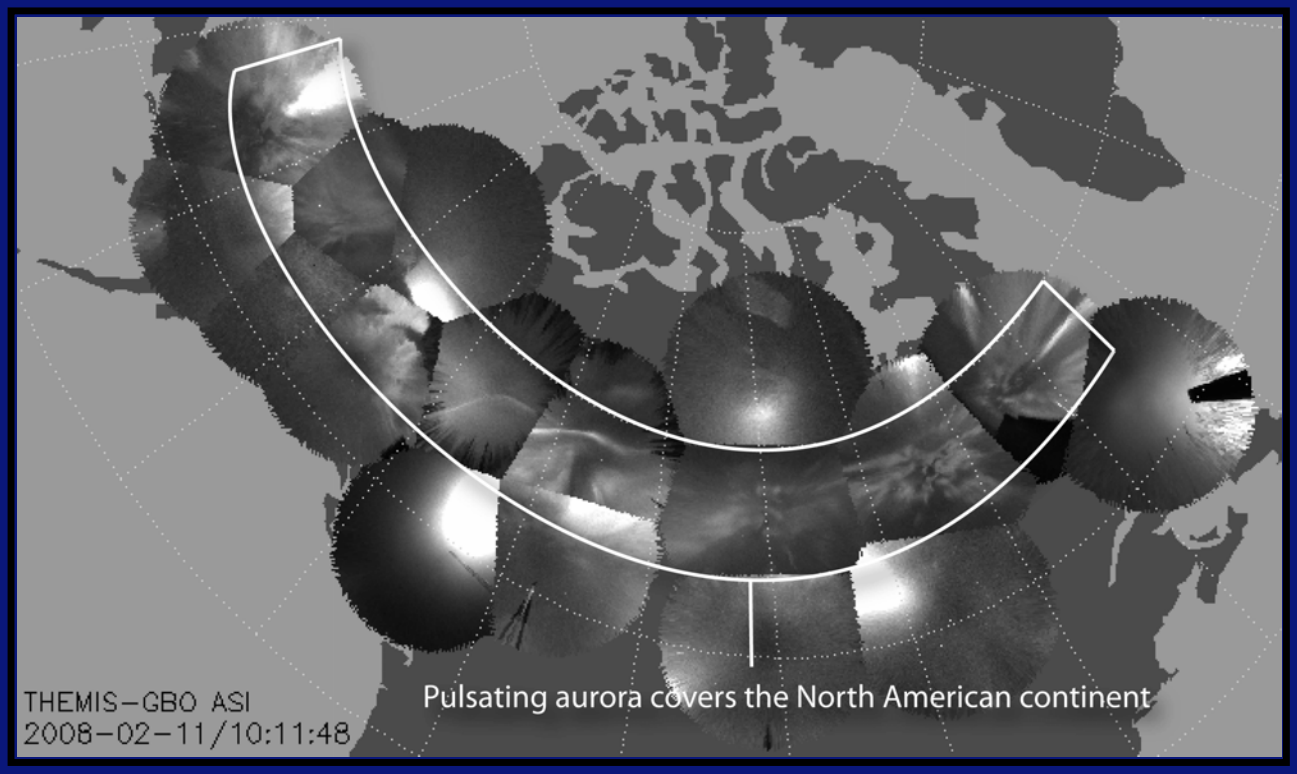

Pulsating auroral events often last for 10 hours or longer and extend across all of North America.

S. L. Jones, M. R. Lessard, K. Rychert, E. Spanswick, E. Donovan, and A. N. Jaynes, Persistent, widespread pulsating aurora: A case study, JGR, *118*, 2998–3006, doi: 10.1002/jgra.50301, 2013. Also see Jones et al., 2011 for statistical results.

Substorm recovery phases
Infrasonic signatures

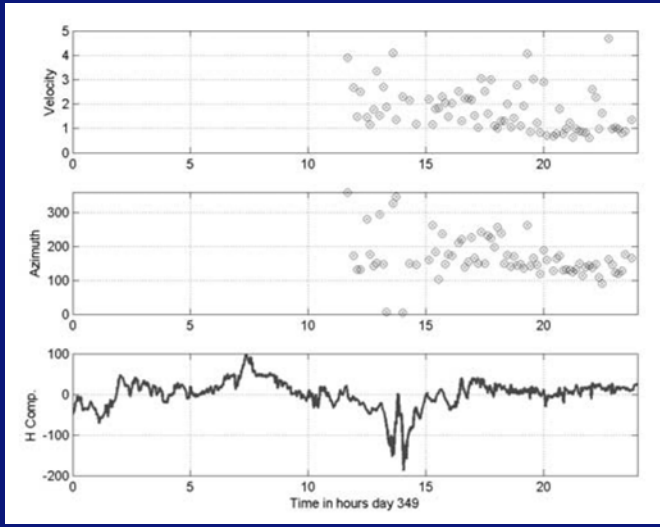

"Data from Day 349, 2002, (December 15) at I53US showing plots of trace-velocity and azimuth estimates of infrasonic signals in the top two panels and the H component of the geomagnetic field at the CIGO magnetic observatory in the bottom panel."

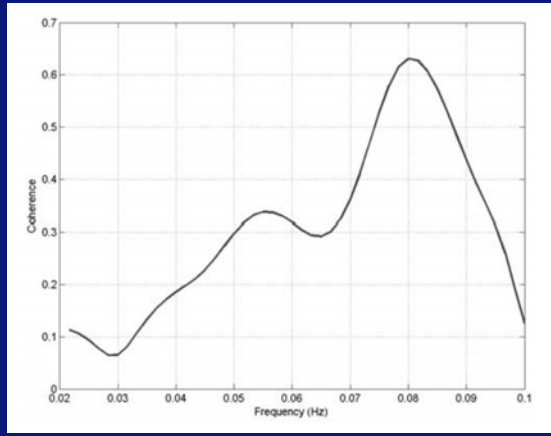

"This plot shows the frequency domain coherence between six minutes of pulsating aurora video data starting at 16:39:33 UT and six minutes of infrasound data starting at 16:44:00 UT. Note that the coherence levels peak near 0.08 Hz."

From: High trace-velocity infrasound from pulsating auroras at Fairbanks, Alaska, Charles R. Wilson, John V. Olson, and Hans C. Stenbaek-Nielsen, GRL, 32, L14810, 2005

Substorm recovery phases
NOx production

- Auroral precipitation may be a significant contributor to thermospheric NO production, which is dependent on the energy flux and duration of the precipitation.
- Pulsating aurora, caused by 10s to 100+ keV electron precipitation (Evans 1987), is frequent, widespead and long lasting.
- Miyoshi et al [2015] showed electron density enhancements down to 68 km using incoherent scatter radar suggesting precipitating energies up to at least 200 keV.
- NO produced at such low altitudes could potentially transport downward and interact with stratospheric ozone (35-40 km).

Miyoshi et al., Energetic electron precipitation associated with pulsating aurora: EISCAT and Van Allen Probe observations, JGR, *120*, 4, 2754–2766, 2015

Substorm recovery phases
NOx production

Simulations show an immediate increase in both ionospheric electron density (top panel) and thermospheric NO enhance-ment (bottom panel) in response to bursts of electron precipitation, particularly in the energy range of 10s of keV. (see Turunen et al. Impact of different energies of precipitating particles on NO_x generation in the middle and upper atmosphere during geomagnetic storms, JASTP, *71*, 10-11, 1176-1189, 2009).

Auroral precipitation is more frequent and longer lasting than REP and SPEs.

Up to *60% of ozone depletion enhancements* (above background levels) at 35-40 km altitude may be due to energetic electron precipitation (Randall et al., Stratospheric effects of energetic particle precipitation in 2003-2004, GRL, *32*, 5, 2005).

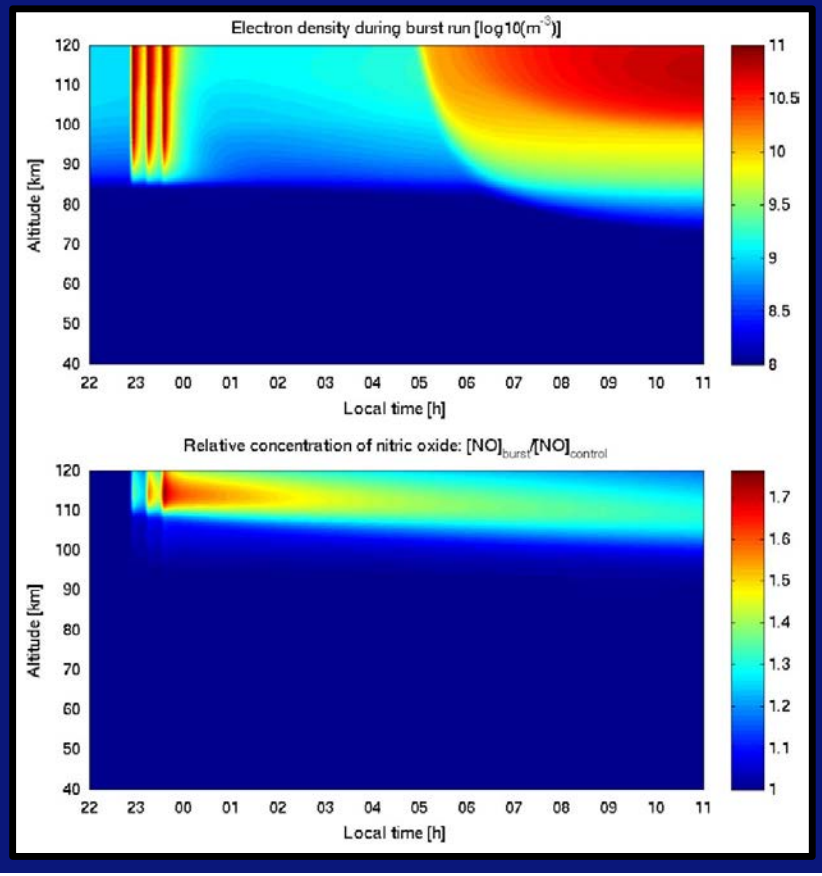

Figure 5. The effect of auroral electron bursts on electron number density and NO concentration. The bursts of electrons have a characteristic energy of 5 keV and a total energy flux of 10 mW m^{-2}. Upper panel: electron number density during the burst run. Lower panel: the behaviour of NO concentration relative to the background level, i.e., the result of the burst run divided by the result of the control run. The electron bursts last 5 min each, starting at 23:05, 23:25, and 23:45 LT.

Cusp aurora
Traveling convection vortices

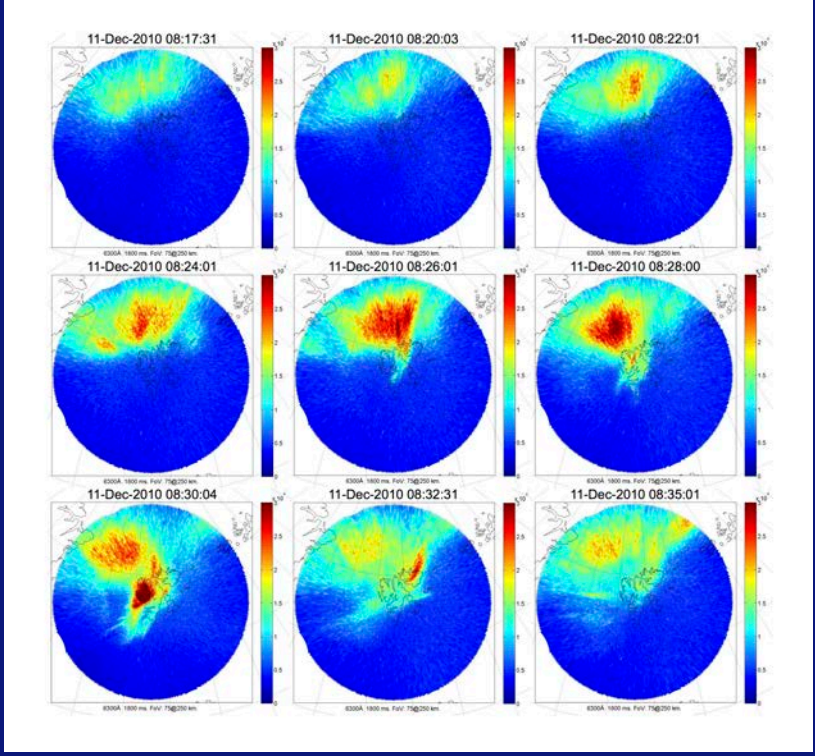

TCVs are thought to be driven by pressure perturbations caused by solar wind buffeting of the magnetosphere. The consequence is a combination of auroral precipitation and an ionospheri tornado, all of which propagates poleward over the polar cap.

All-sky camera images at 630 nm at a 2-minute cadence, acquired during the TCV event on Dec 11, 2010. The emissions occurring poleward of the station before the event are thought to be cusp precipitation. The emissions associated with the TCV are the brief, bright spots directly over Longyearbyen.

Mutli-Point Observations of Traveling Convection Vortices: Ionosphere-Thermosphere Coupling
H. Kim, M. R. Lessard, S. L. Jones, K. Lynch, P. Fernandes, J. Moen, K. Oksavik, T. Yeoman, A. Aruliah, M. Engebretson, and J. Posch

Cusp aurora
Traveling convection vortices

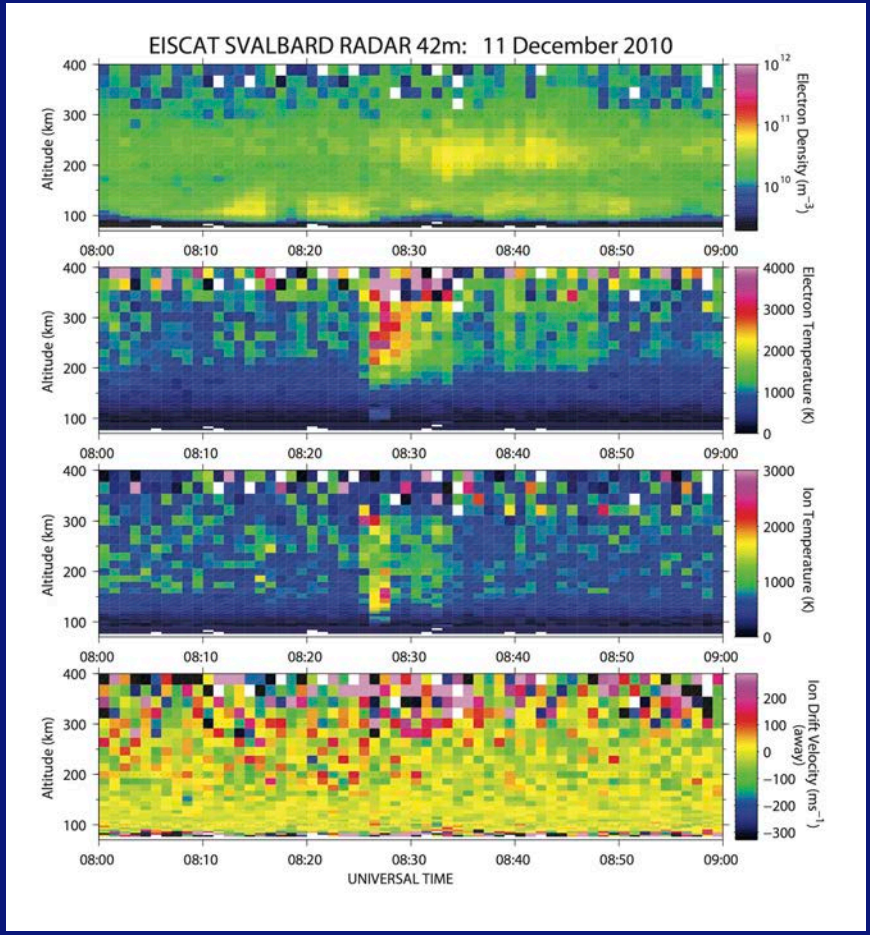

EISCAT observations of the TCV, showing the combination of both Joule heating and soft precipitation.

Panel 2 shows enhanced electron temperature (Te) above 150 km altitude. There is no E-region, so the precipitation must be soft.

Panel 3 shows enhanced ion temperature (Ti), consistent with Joule heating. The Joule heating starts at 08:26 UT, which is exactly when the aurora first appears in the EISCAT beam, implying that there are strong electric fields associated with the onset of this aurora.

Cusp aurora
Traveling convection vortices

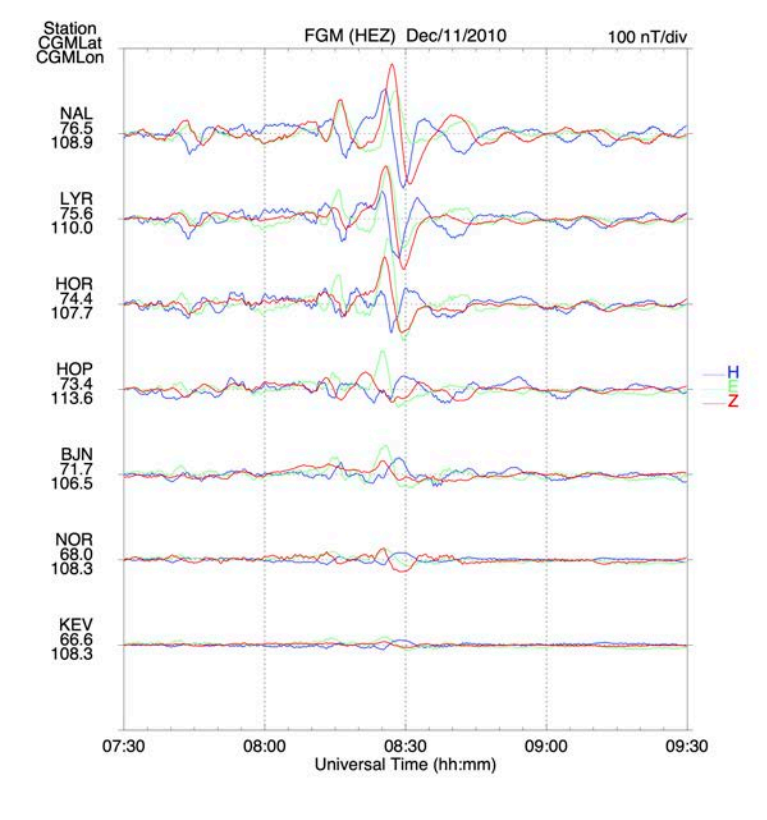

Magnetometer data from the IMAGE magnetometer network, showing the passage of the TCV starting at ~08:20.

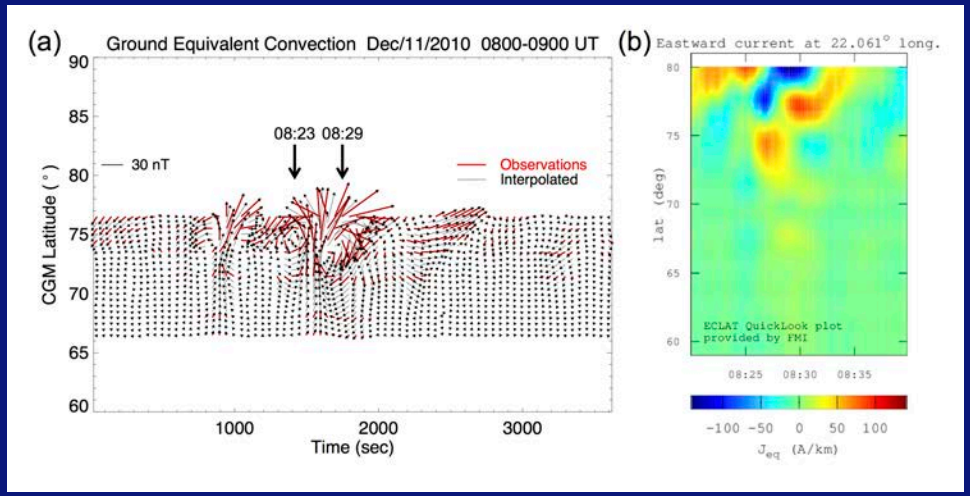

Latitudinally interpolated convection vectors are displayed as black lines overplotted with the observed convection patterns in red lines. The centers of each convection vortex are indicated by the arrows at 08:23 and 08:29 UT, respectively. The 2D equivalent current plot is generated by the online tool provided by the IMAGE Network website at http://space.fmi.fi/MIRACLE/iono 2D.php.

Cusp aurora
Traveling convection vortices

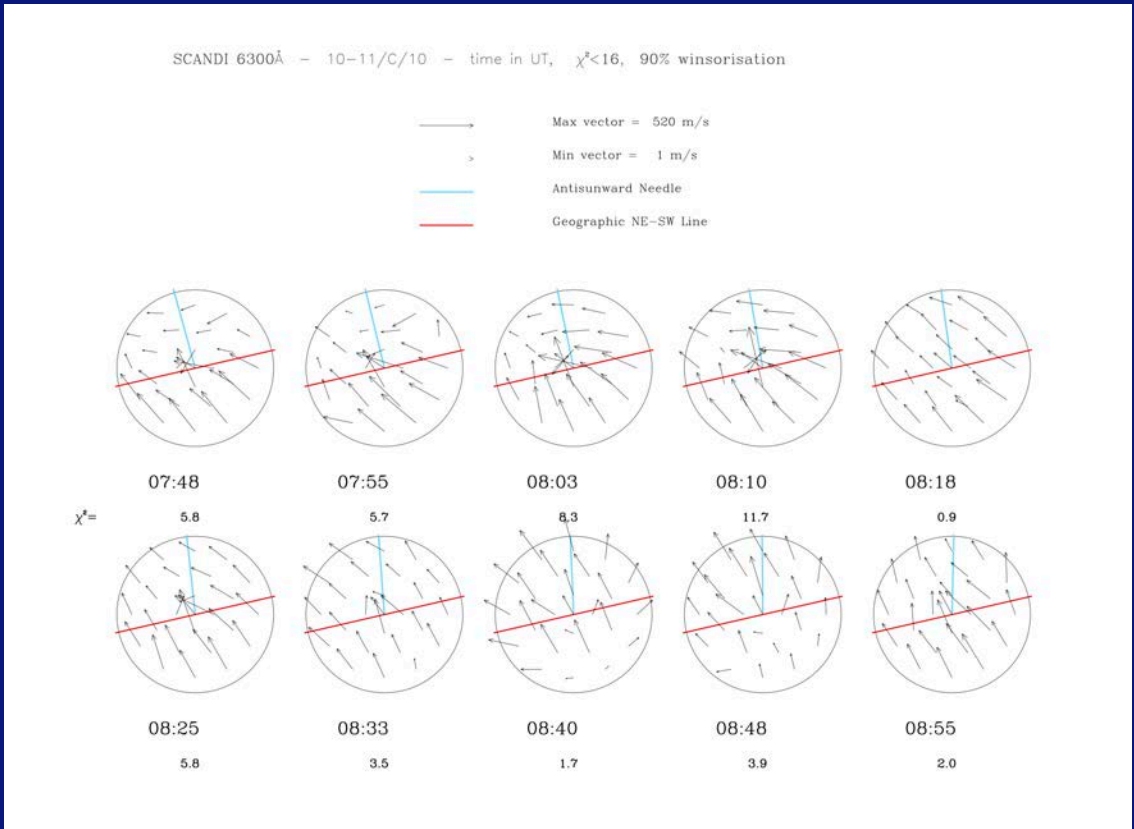

SCANDI observations of neutral winds over Longyearbyen. Before the TCV passed, winds were quite uniform. Beginning near 08:33 UT, winds equartorward of the station decrease significantly, followed by a clear divergence in the 08:40 UT image.

Cusp aurora
Speed bumps in space..

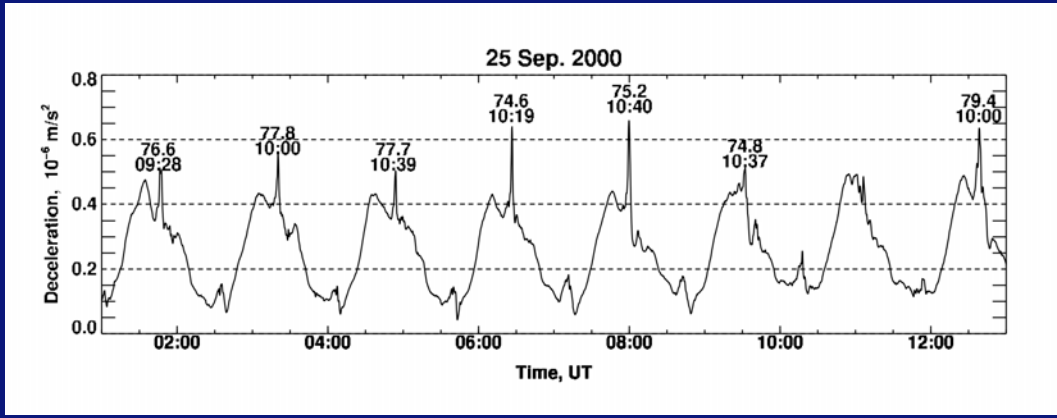

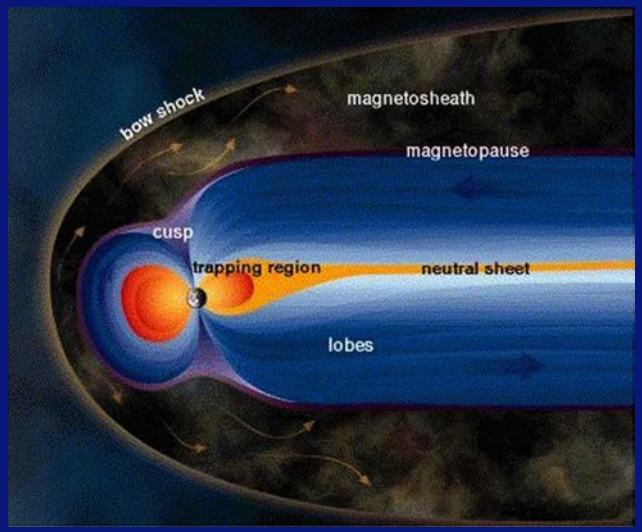

Plot showing 8 orbits of the CHAMP satellite, at 400 km altitude, nearly polar inclination. Vertical axis shows accelerometer data, with narrow spikes (“bumps”) in the vicinity of the cusp region.

Spikes are observed in conjunction with small-scale currents (observed by the magnetometer), e.g., electron precipitation and, presumably, aurora.

Luhr et al., Thermospheric up-welling in the cusp region: Evidence from CHAMP observations, Geophys. Res. Lett., 31, 6805, 2004.

Cusp aurora
Speed bumps in space..

G. N. Kervalishvili and H. Luhr, The relationship of thermospheric density anomaly with electron temperature, small-scale FAC, and ion up-flow in the cusp region, as observed by CHAMP and DMSP satellites, Ann. Geophys., 31, 541–554, 2013:

1. The mean amplitude of the prominent relative density enhancement peak shows no seasonal variations and amounts to enhancements of ~1.33.

2. There is a linear relationship between Vz and Te, with only a slight variation from season to season. FAC tend to increase during summers, though electron temperatures decrease during these times.

S. Rentz and H. Luhr, Climatology of the cusp-related thermospheric mass density anomaly, as derived from CHAMP observations, Ann. Geophys., 26, 2807–2823, 2008

1. Signatures are stronger in the northern hemisphere.

2. Solar zenith angle appears to play only a minor role

Cusp aurora
Speed bumps in space..

S. Rentz and H. Luhr, Climatology of the cusp-related thermospheric mass density anomaly, as derived from CHAMP observations, Ann. Geophys., 26, 2807–2823, 2008

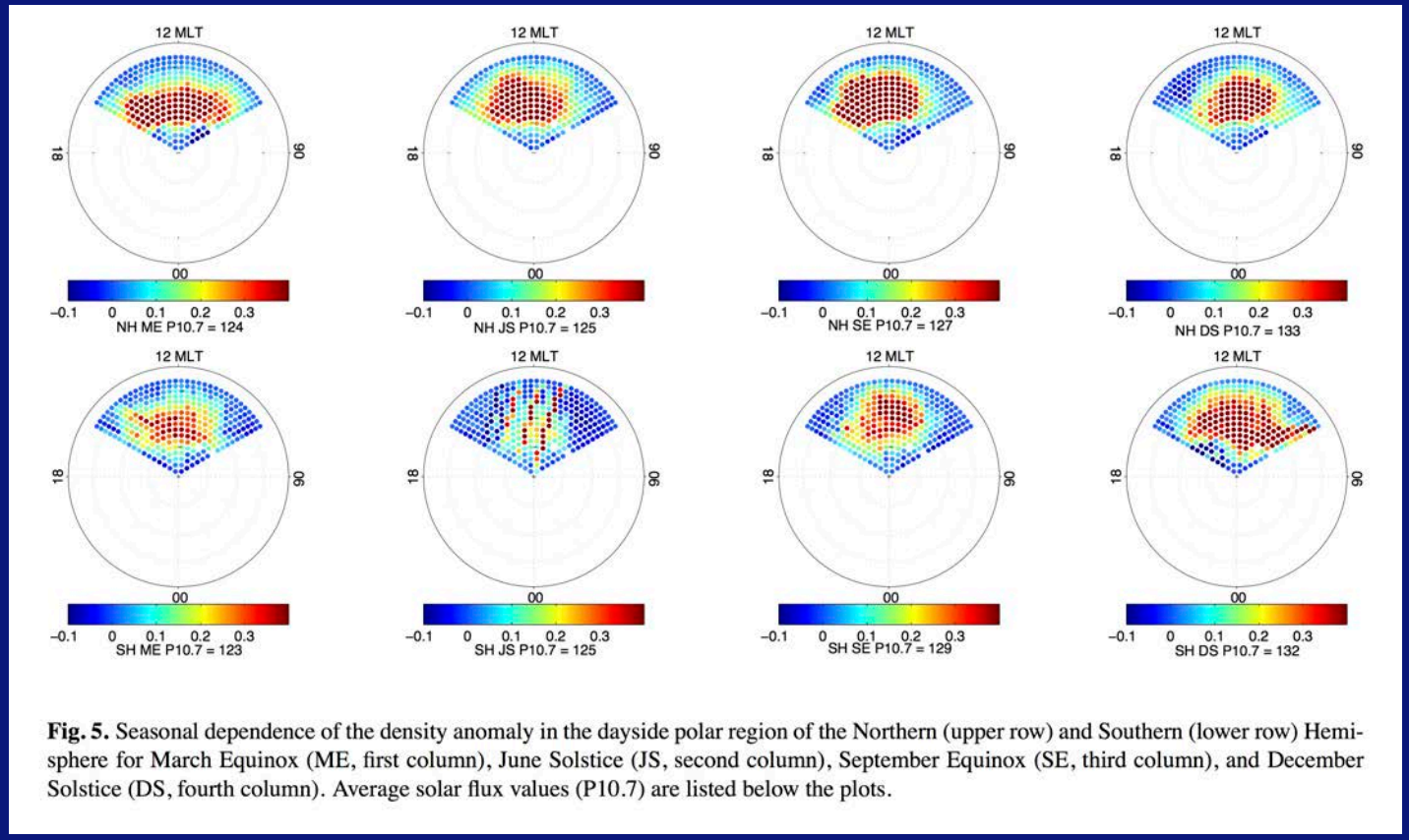

Fig. 5. Seasonal dependence of the density anomaly in the dayside polar region of the Northern (upper row) and Southern (lower row) Hemisphere for March Equinox (ME, first column), June Solstice (JS, second column), September Equinox (SE, third column), and December Solstice (DS, fourth column). Average solar flux values (P10.7) are listed below the plots.

About those strong field-aligned currents…

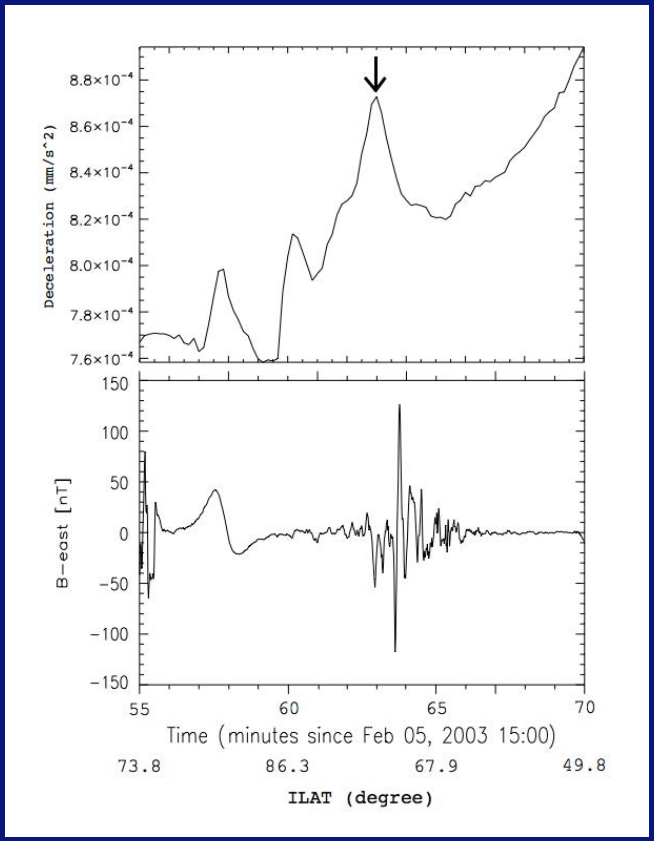

The lower panel shows the east-west component of the magnetometer data, with small-scale field-aligned currents observed from 1603 to 1605 UT (roughly 74 to 69 ILAT).

Note that the displacement between the neutral bump and the FAC is due to field-line dip angle.

The upwelling events are well-correlated with small-scale currents, but this point has not been seen as very important (beyond the original Luhr paper).

Related work

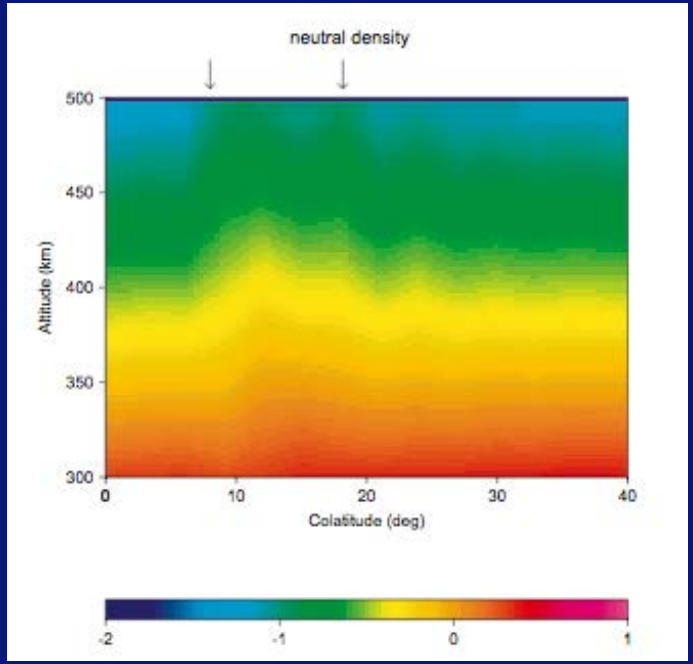

Demars and Schunk [2007] use MSIS and IRI models in order to replicate the CHAMP observations of density enhancements a factor of 1.8 at 400 km altitude, the heating needs to be increased by a factor of 110 over the background, driving the ion temperature up from the nominal 1000 K to more than 10,000 K in the cusp region. This is not really a realistic situation.

Related work

Neutral density enhancements in the southern cusp by the Streak satellite (at 250 km) show small density *depletions.* If the speed bumps (observed at ~450 km altitude) are driven by Joule heating in the E-region, depletions at this altitude would not be expected

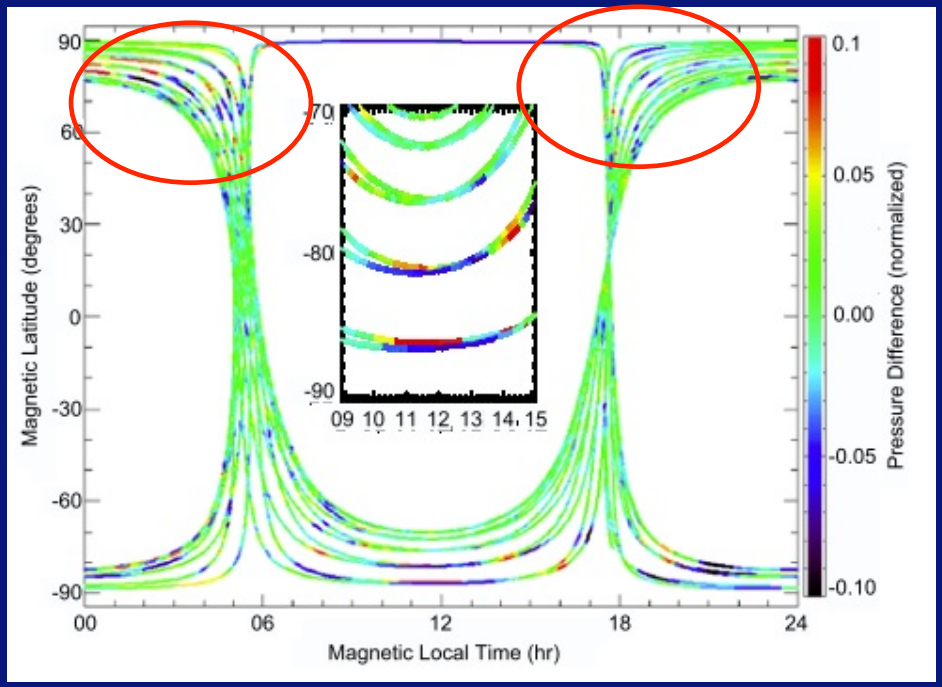

Deviations from the predictions of the MSIS model on 2 Mar 2006

Clemmons, J. H., J. H. Hecht, D. R. Salem, and D. J. Strickland (2008), Thermospheric density in the Earth's magnetic cusp as observed by the Streak mission, Geophys. Res. Lett., 35, L24103, doi: 10.1029/2008GL035972.

Atmospheric and ionospheric profiles

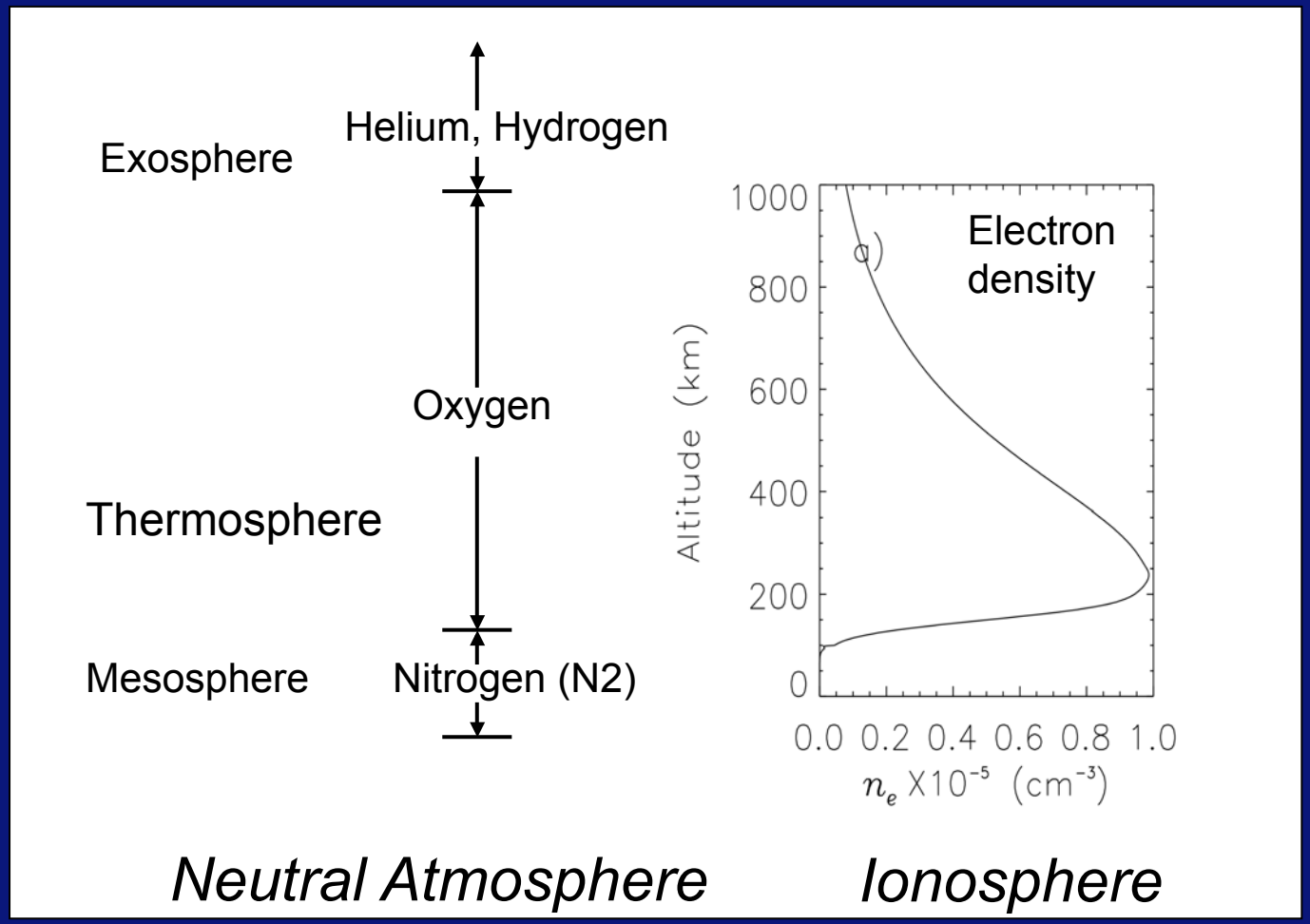

The upper atmosphere becomes stratified at “high” altitudes due to the lack of collisions. A result is that neutral upwelling generally refers to atomic oxygen.

Is upwelling driven by Joule heating *or* by soft electron precipitation (and/or strong FAC)?

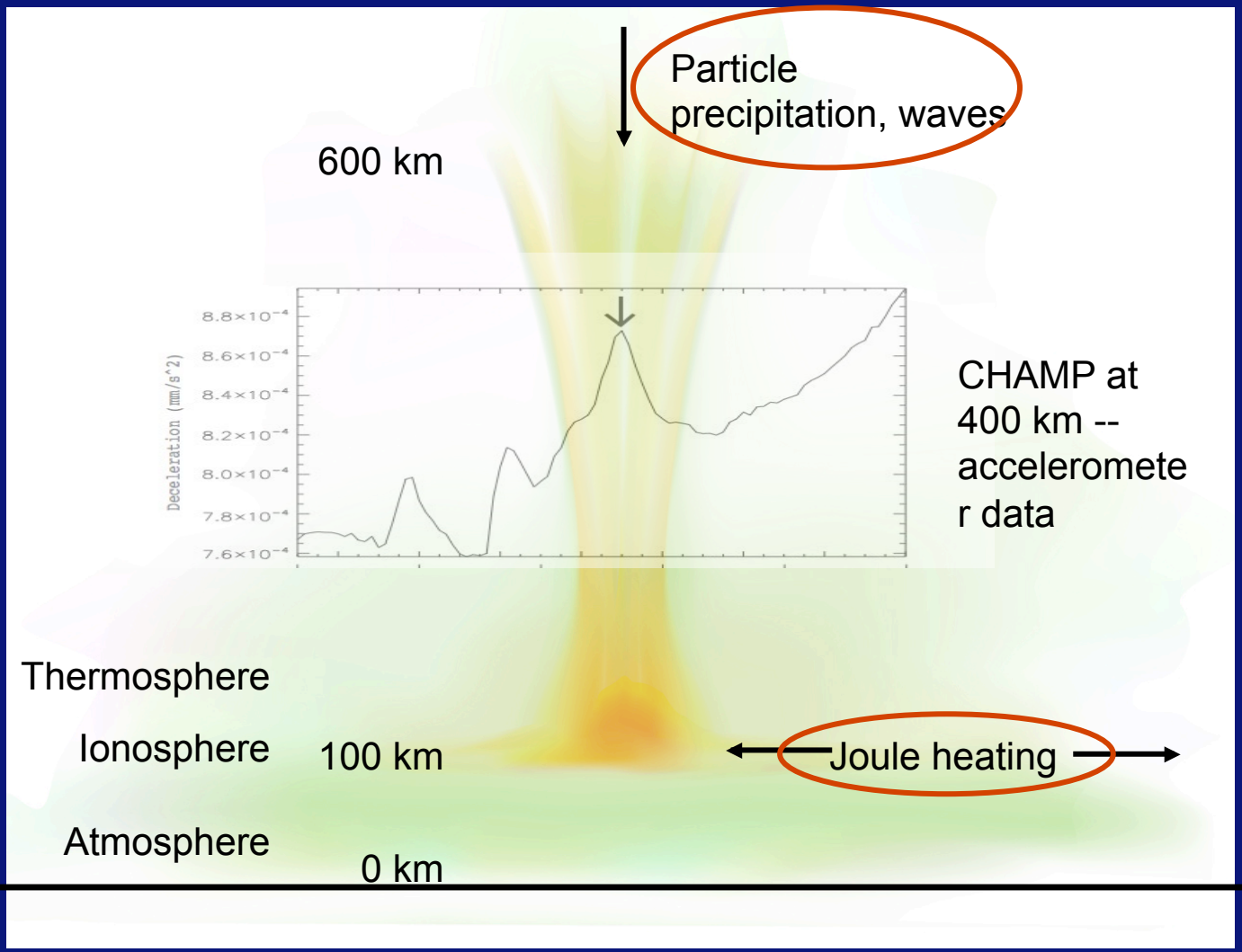

Rocket Experiment for Neutral Upwelling 2 (RENU2)

Launch an appropriately instrumented sounding rocket through the cusp region (e.g., over Svalbard) during an event with soft electron precipitation and Joule heating. Include relevant ground observations.

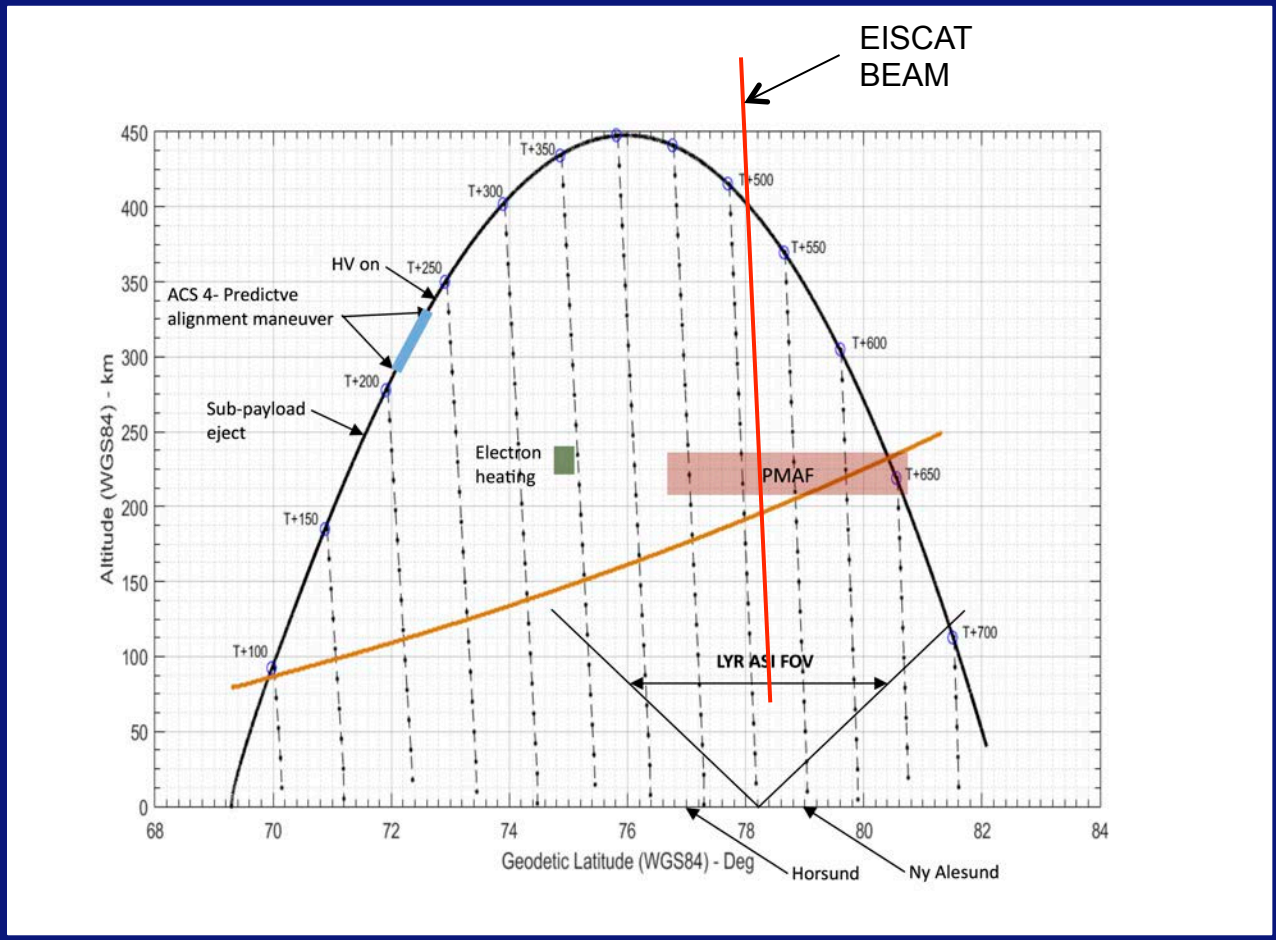

Relevant processes that we are aware of

- Joule heating heats the thermosphere at altitudes near 100 km and causes neutral upwelling.

- Joule heating also heats the ionosphere in this region and likewise causes it to expand vertically. This is one of two mechanisms that contribute to the lower altitude stages of “ion upflow”. This is “Type 1” upflow.

- The other mechanism starts with soft (100 eV) electron precipitation, which heats the very cold ambient ionospheric electrons. The heated electrons expand upwards, lifting ions as they do so. This is “Type 2” upflow.

- In either case, BBELF waves at higher altitudes (400-600 km) can cause the ions to reach escape velocity, launching them into the magnetosphere. This is then called “ion outflow”..

Proposed theories for small-scale neutral upwelling

1. G. Crowley: The upwelling is fundamentally driven by Joule heating

Crowley, G., D. J. Knipp, K. A. Drake, J. Lei, E. Sutton, and H. Lühr (2010), Thermospheric density enhancements in the dayside cusp region during strong BY conditions, Geophys. Res. Lett., 37, L07110, doi: 10.1029/ 2009GL042143.

2. A. Otto: The upwelling is driven as part of the “Type 2” ion outflow process

Sadler, F. B., M. Lessard, E. Lund, A. Otto and H. Lühr (2012), Auroral precipitation/ion upwelling as a driver of neutral density enhancement in the cusp, Journal of Atmospheric and Solar-Terrestrial Physics 87–88.

3. B. Zhang: Soft electron precipitation enhances conductivities in F-region, which enables increased Joule heating at these altitudes.

Zhang, B., W. Lotko, O. Brambles, M. Wiltberger, W. Wang, P. Schmitt, and J. Lyon (2012), Enhancement of thermospheric mass density by soft electron precipitation, Geophys. Res. Lett., 39, L20102, doi: 10.1029/2012GL053519.

4. D. Brinkman (and J. Clemmons): Direct particle heating plays a major role, works with higher altitude Joule heating

Brinkman, D. G., R. L. Walterscheid, J. H. Clemmons and J. H. Hecht (2016), High-resolution modeling of the cusp density anomaly: Response to particle and Joule heating under typical condi- tions, J. Geophys. Res. Space Physics, 121, 2645-2661, doi:10.1002/2015JA021658.

Proposed RENU2 observations

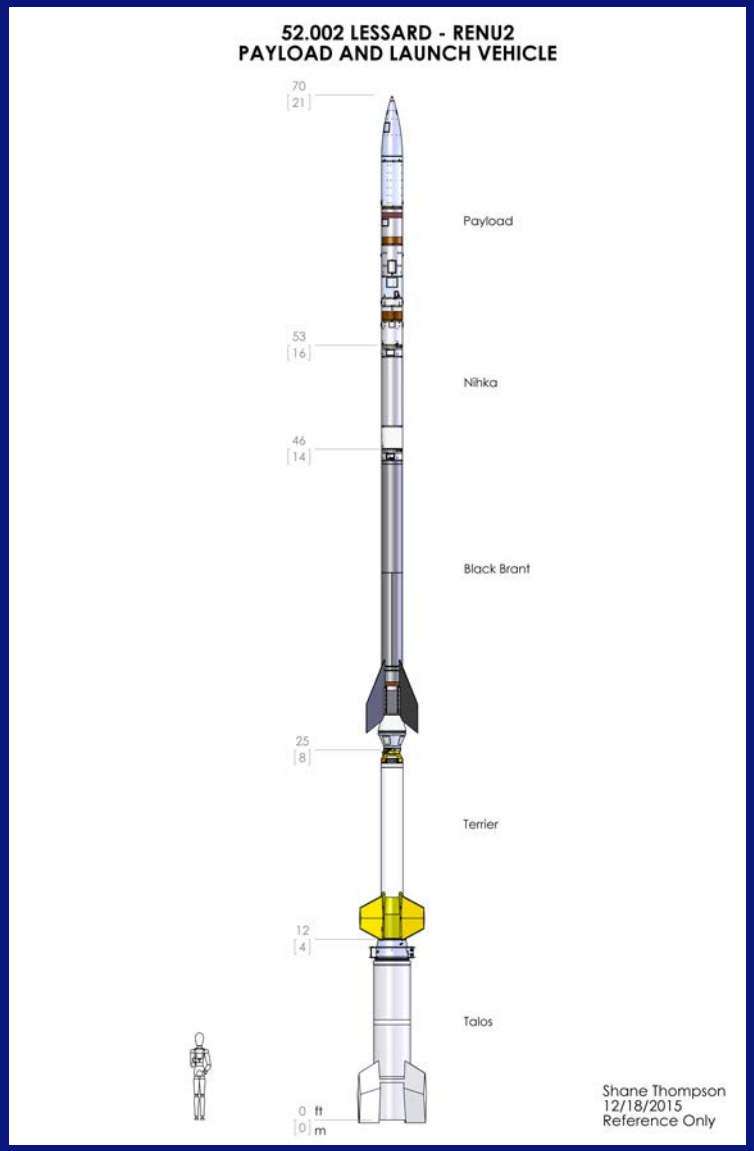

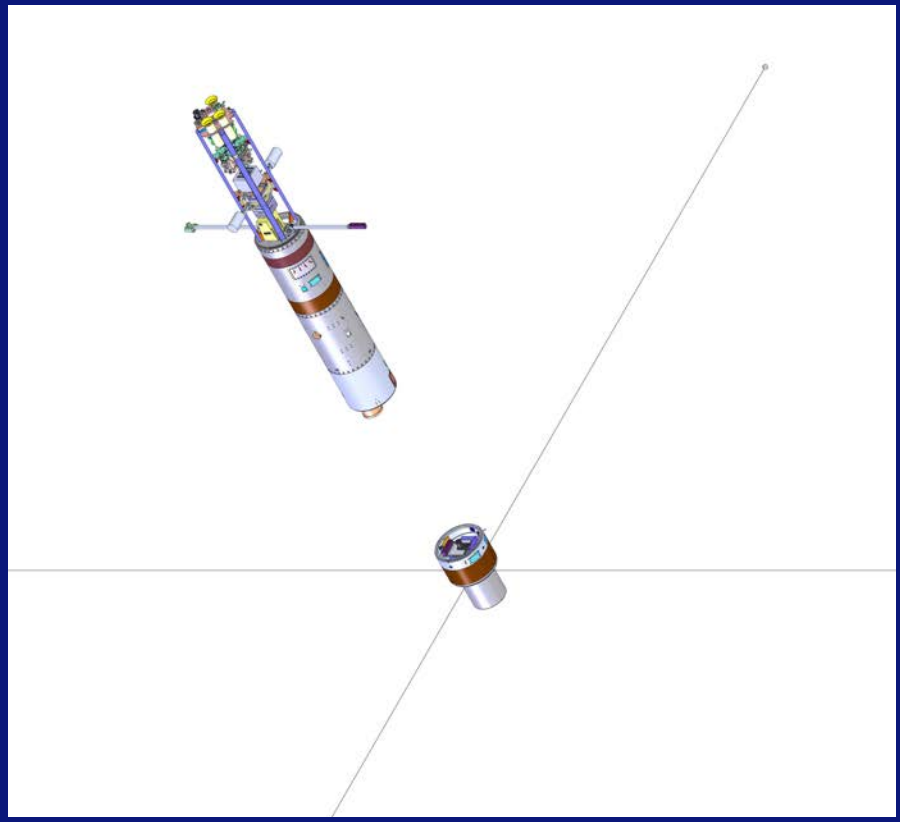

Total Weight = 11,276 lb
Total Length = 70 feet

Proposed RENU2 observations

Instrumentation

Instrument	Institution	Measurement	Range
Ion Gauges	Aerospace	Neutral density and temp	$\geq 10^{-10}$ T
PMTs	Aerospace	N_2^+ (391.4 nm), O (630.0, 844.6 nm)	30 cts/s/R
EPLAS	UNH	3D distributions, precip. electrons	6 eV - 15 keV
HT - Thermal ions	Dartmouth	3D distributions, ambient ions	0.06-3 eV
HM - SuperT Ions	Dartmouth	3D, upflowing ions	6-800 eV
BEEPS - Ion mass	Dartmouth	3D, upflowing O^+, H^+	6-800 eV
Ion Mag Spec	Aerospace	???	??
ERPA (2)	UNH	Cold electron temps (and density?)	0.06 - 3 eV
COWBOY E-Fields	Cornell	Onboard electric fields	0-20 kHz, 0-1000 Hz
Billingsley mag	Cornell	3-axis fluxgate	$\pm 60,000$ nT
Racetrack Mag	UNH	3-axis fluxgate, 24-bit (30 pT)	$\pm 60,000$ nT
Imager	UNH	630 nm images, below the payload	
UV-PMT	UNH	O (130.4 nm), 12° FOV, above	TBD

Table 1: RENU2 instruments and quantities measured.

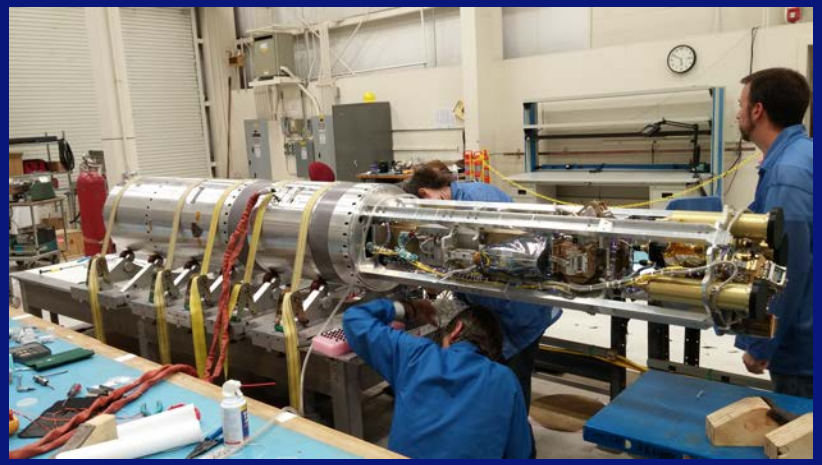

RENU2 Launch

Context – solar wind observations

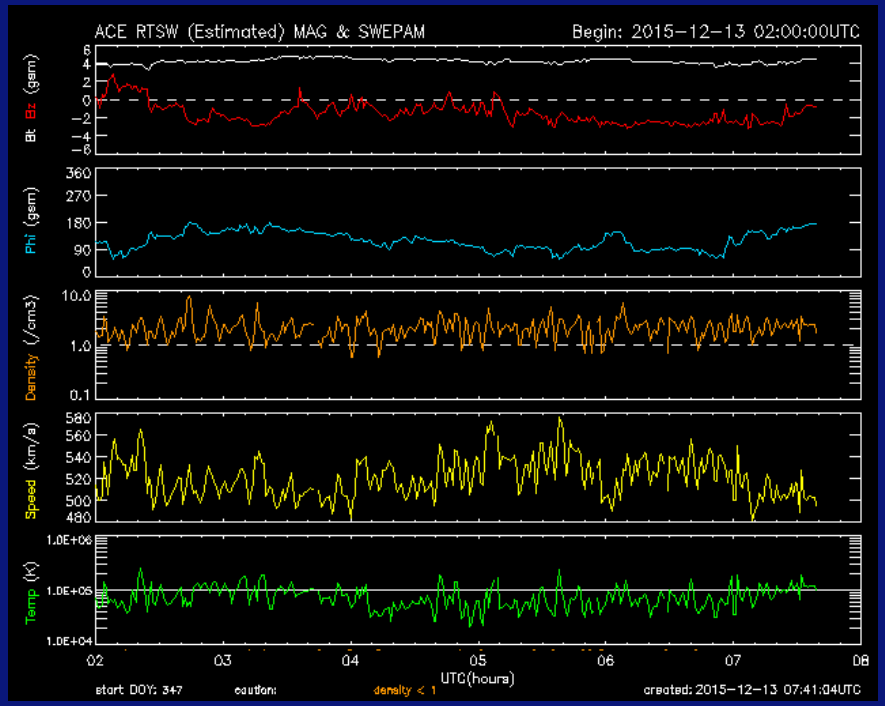

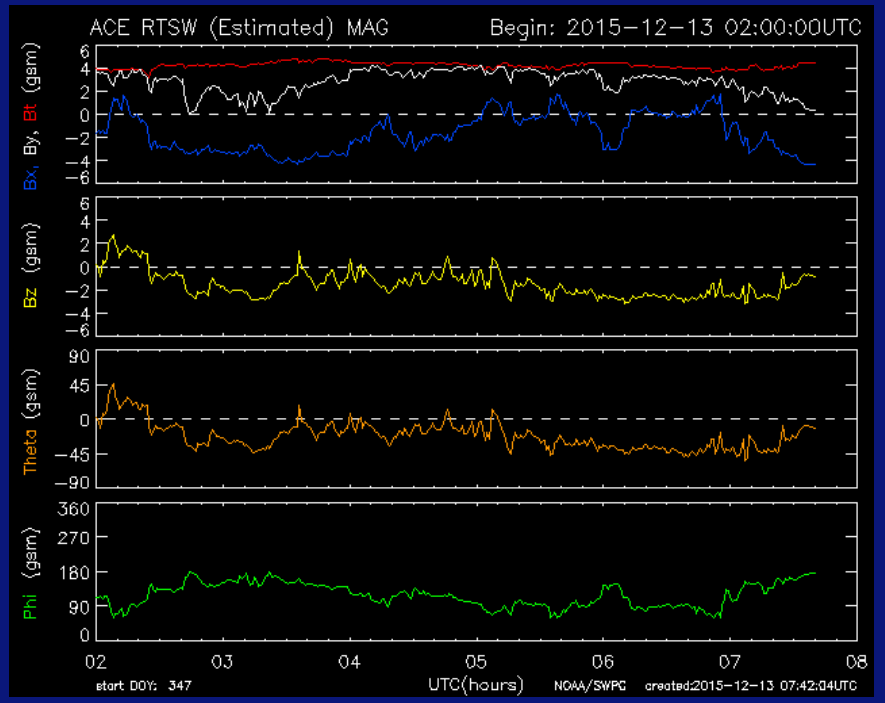

Data from the ACE satellite at L1. Note negative Bz and positive By; typical density but high solar wind speed. Estimated propagation time of approximately 50 minutes.

RENU2 Launch

Context – Cutlass (SuperDARN) radar

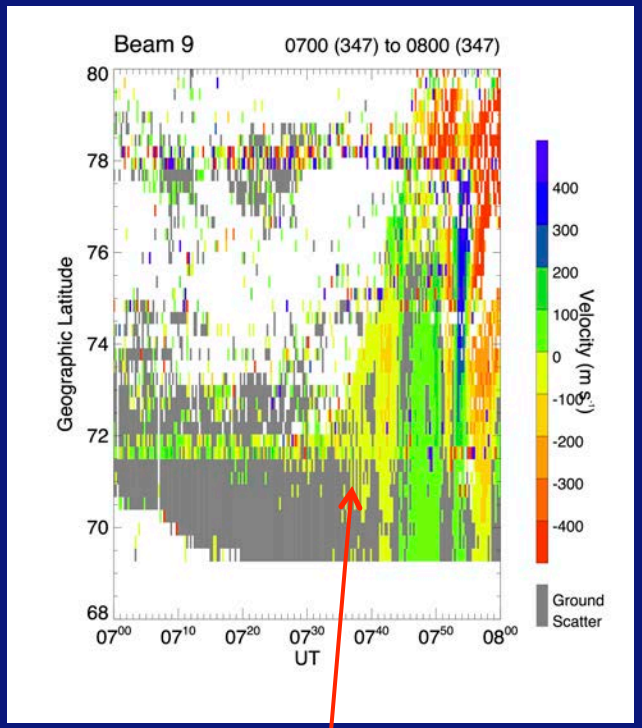

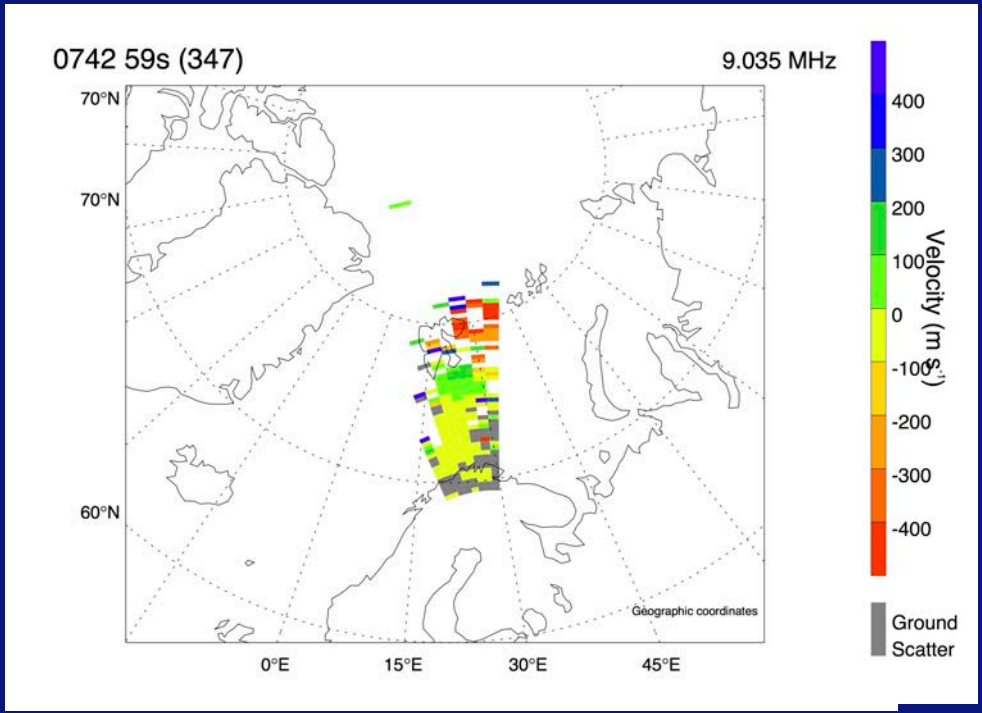

Evidence from Finland of our rotation into the cusp – the onset of poleward ionospheric flows. Launch was at 07:34 UT.

A 2-D snapshot of radar observations confirming that “we are in the cusp”, 9 minutes after launch

RENU2 Launch

Context – EISCAT radar

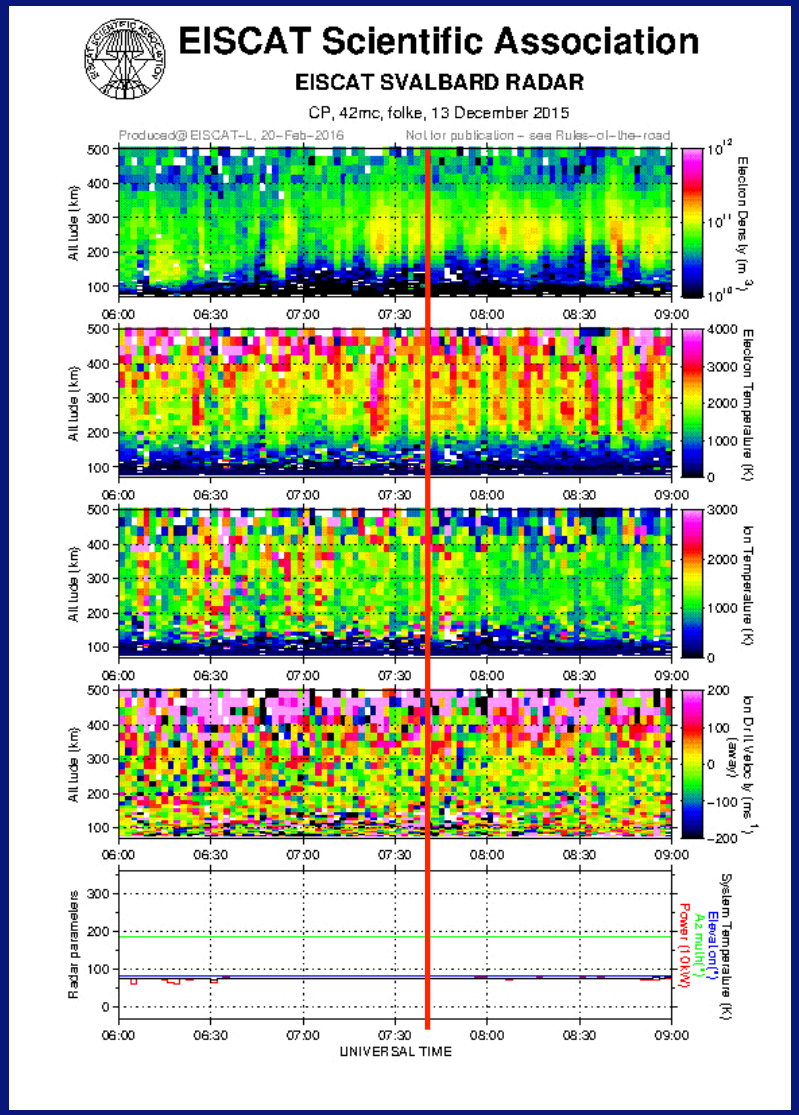

1) Several transient enhancements in the electron density in F-region (consistent with the cusp).

2) Several transients in electron temperature, which would be consistent with PMAF activity

3) Joule heating mostly seen in the hour prior to launch, but maybe some weak Joule heating around 07:38 - 07:48 UT.

4) Weak ion upflow in topside region (above 400 km altitude) throughout. Around 07:34 - 07:48 UT, ion upflow appears to have been extending all the way down to 300 km altitude.

RENU2 Launch

Context – allsky camera data

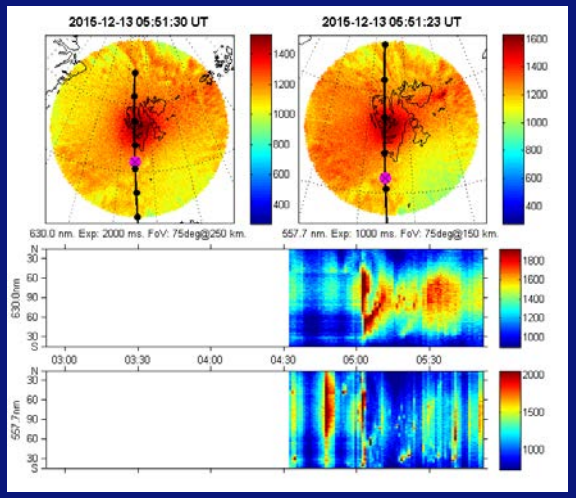

5:51:30

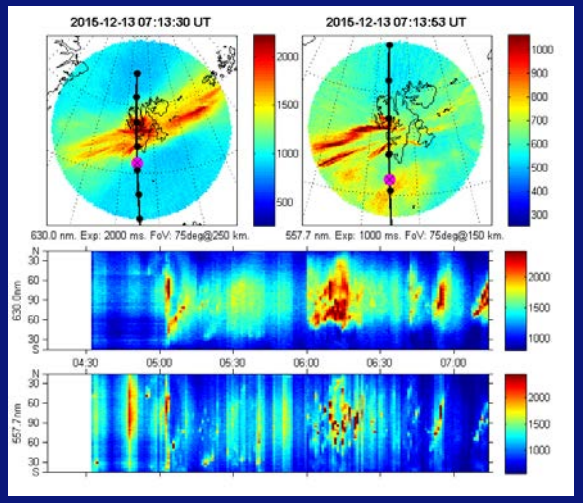

7:13:30

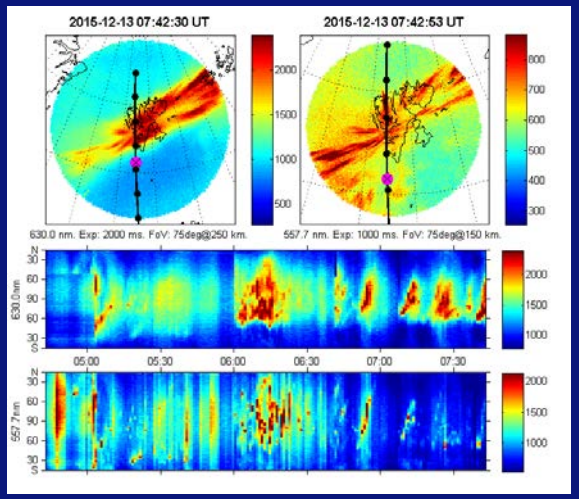

7:42:30

RENU2 Launch

Context

Notes:
5:45 “snow falling hard”
6:08 “less snow, seeing stars”
6:48 “inside the cusp?”
6:58 “clearing snow from domes”
7:00 take the clock to T-15:00
7:14 Drop from T-15:00 to T-2:00
7:27 Hold at T-2:00
7:32 Pick up the count
7:34 LAUNCH!

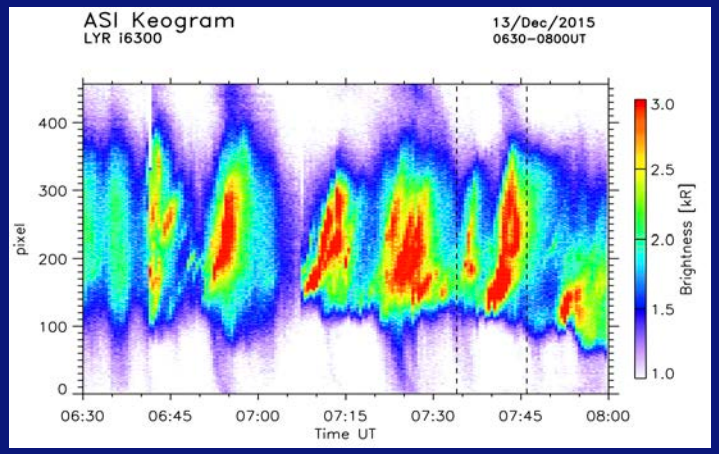

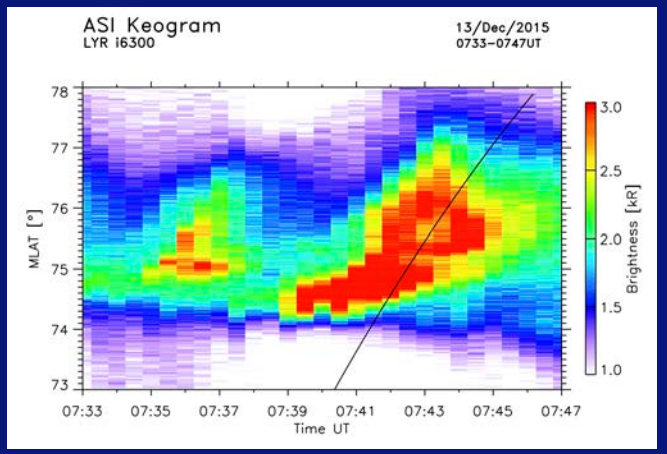

RENU2 Launch

Context – what is a PMAF?

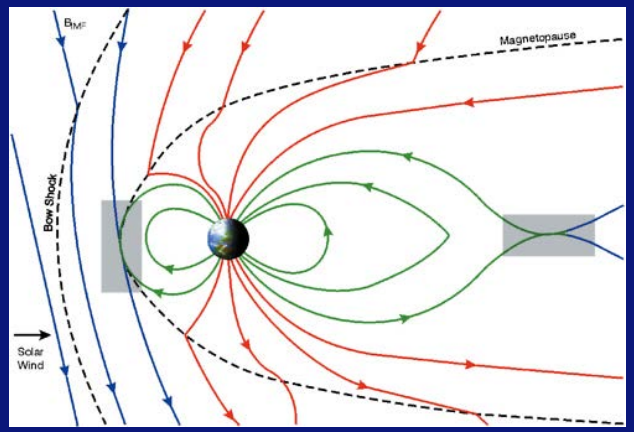

Credit NAP: dayside reconnection drives PMAFs and stepped ions

Notes:
-- Field aligned precipitation
-- Electron energies of ~100 eV
-- Poleward propagation the order of 1 km/s.

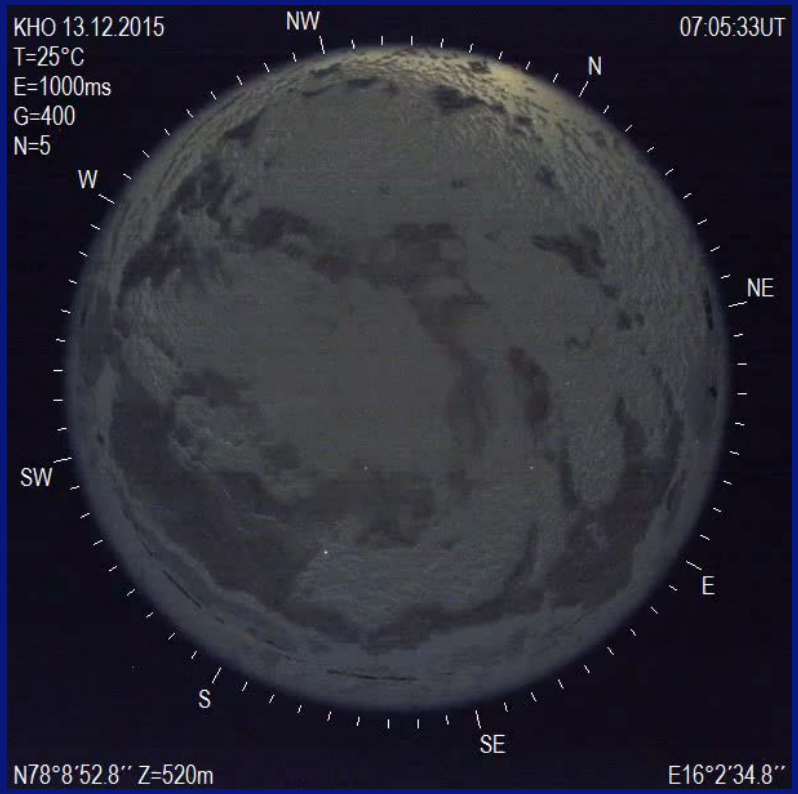

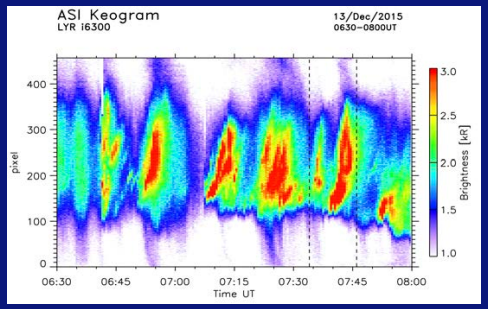

RENU2 Electrons

Data – electron precipitation

Apogee of 447 km at T+409

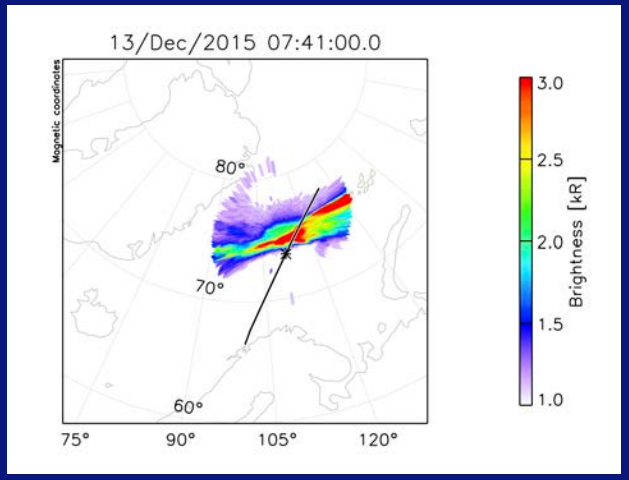

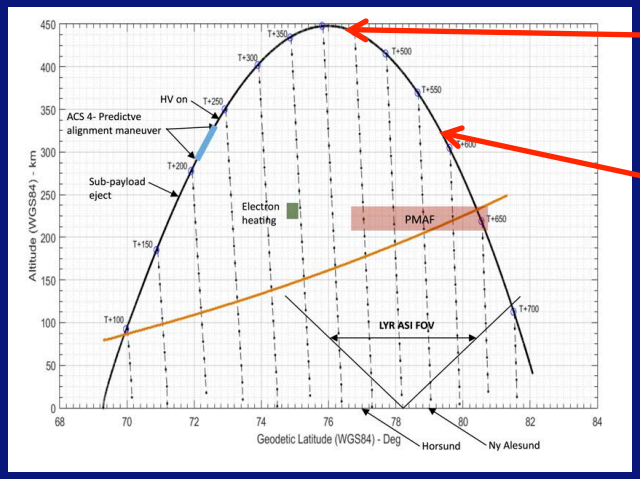

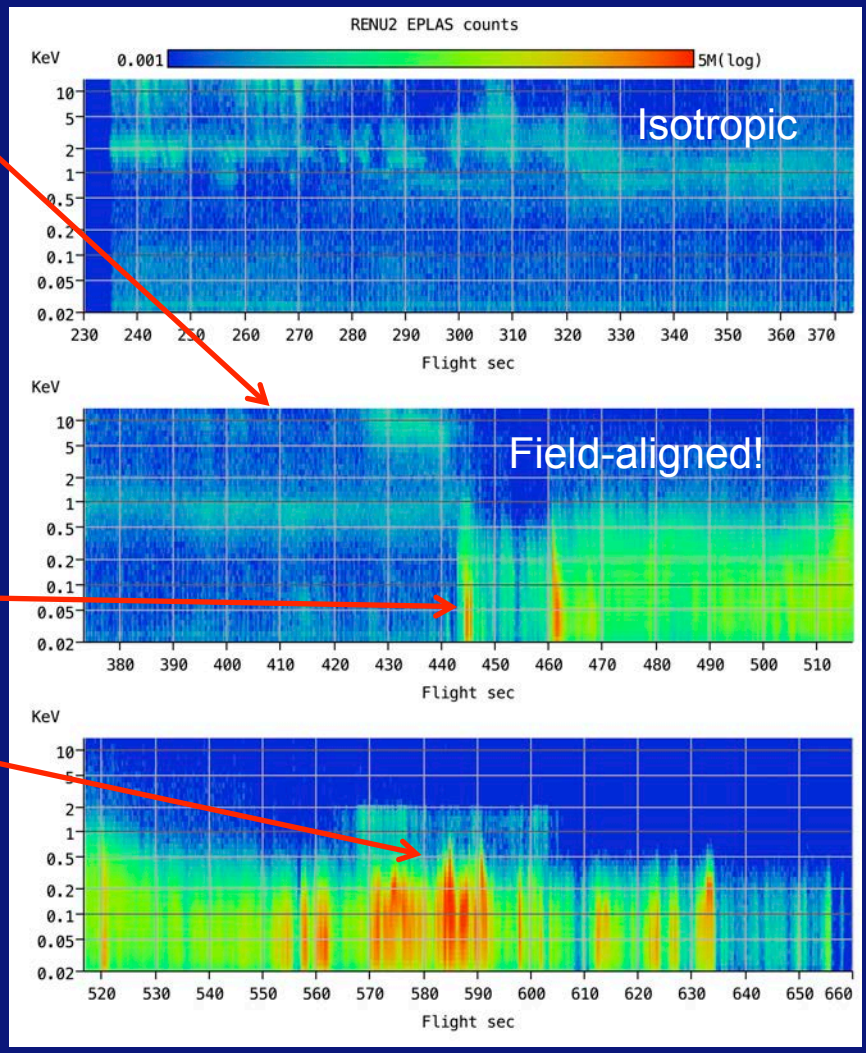

RENU2 Ions (Dartmouth)

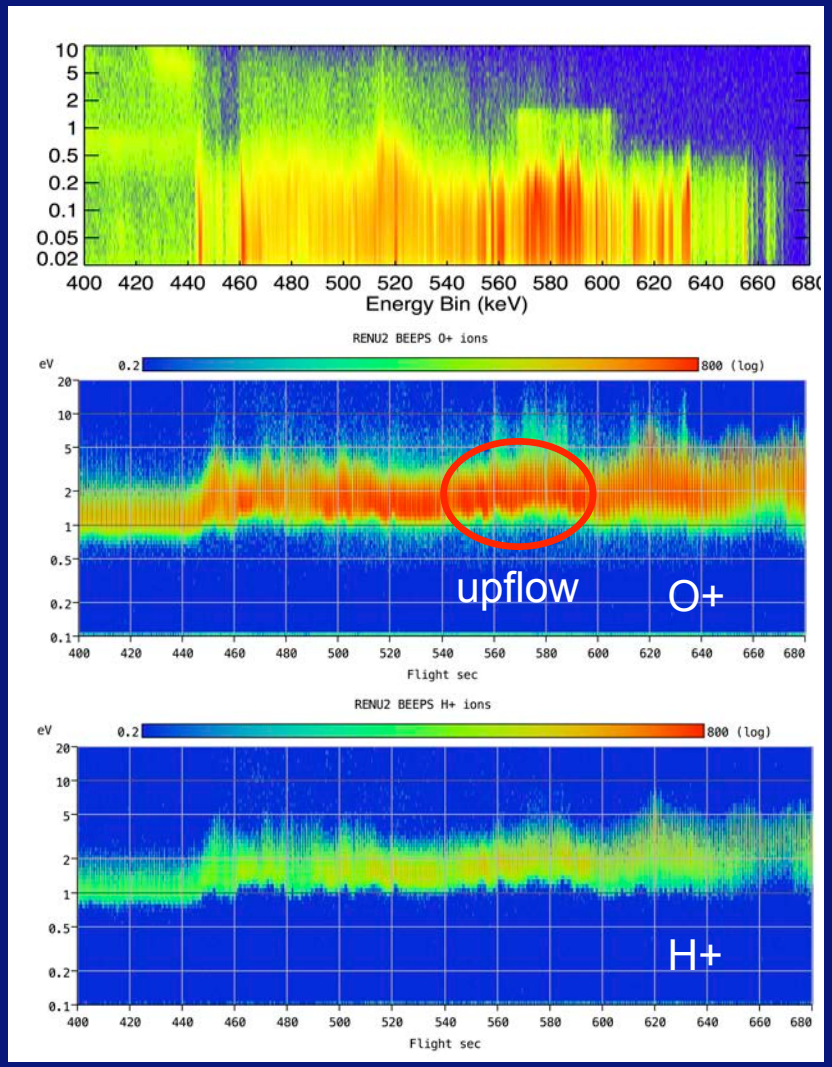

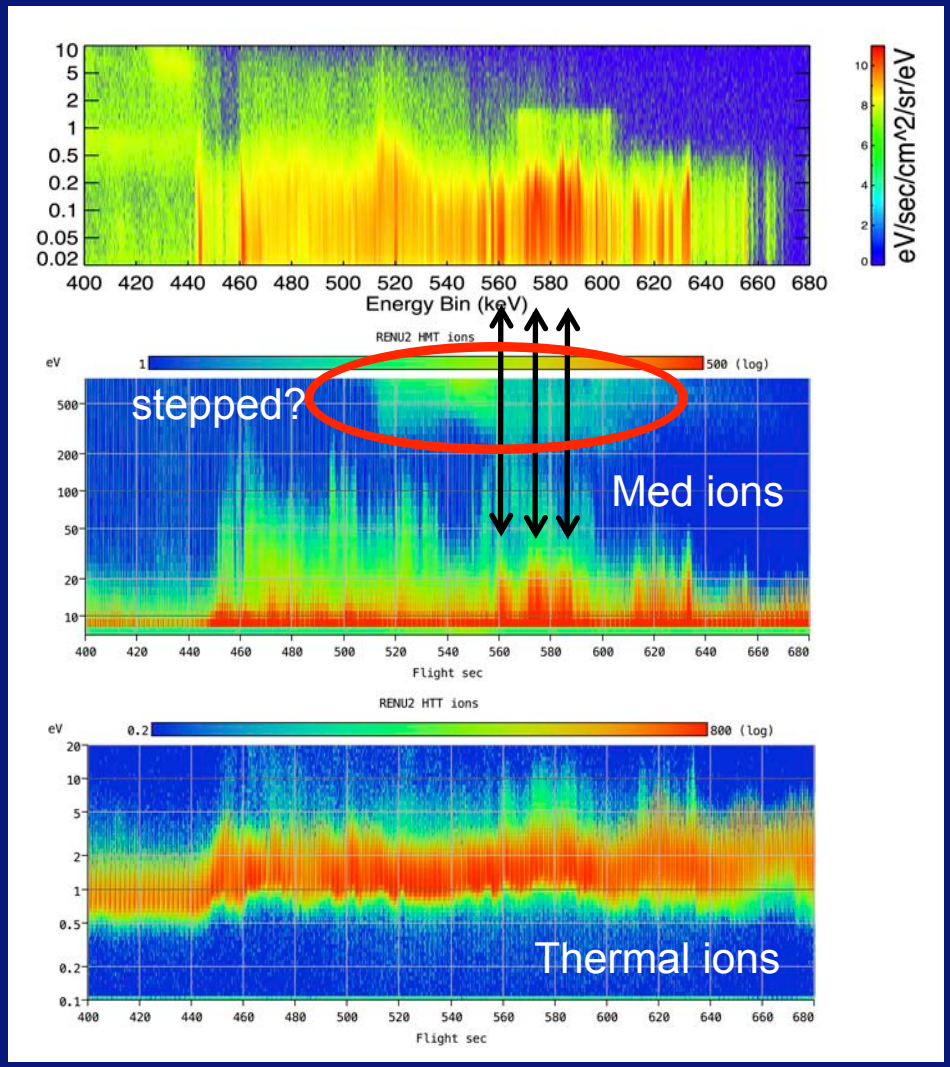

J. Lunde et al., Ion-dispersion and rapid electron fluctuations in the cusp: a case study, Ann. Geophys., 26, 2485–2502, 2008

RENU2 Ions (Dartmouth)

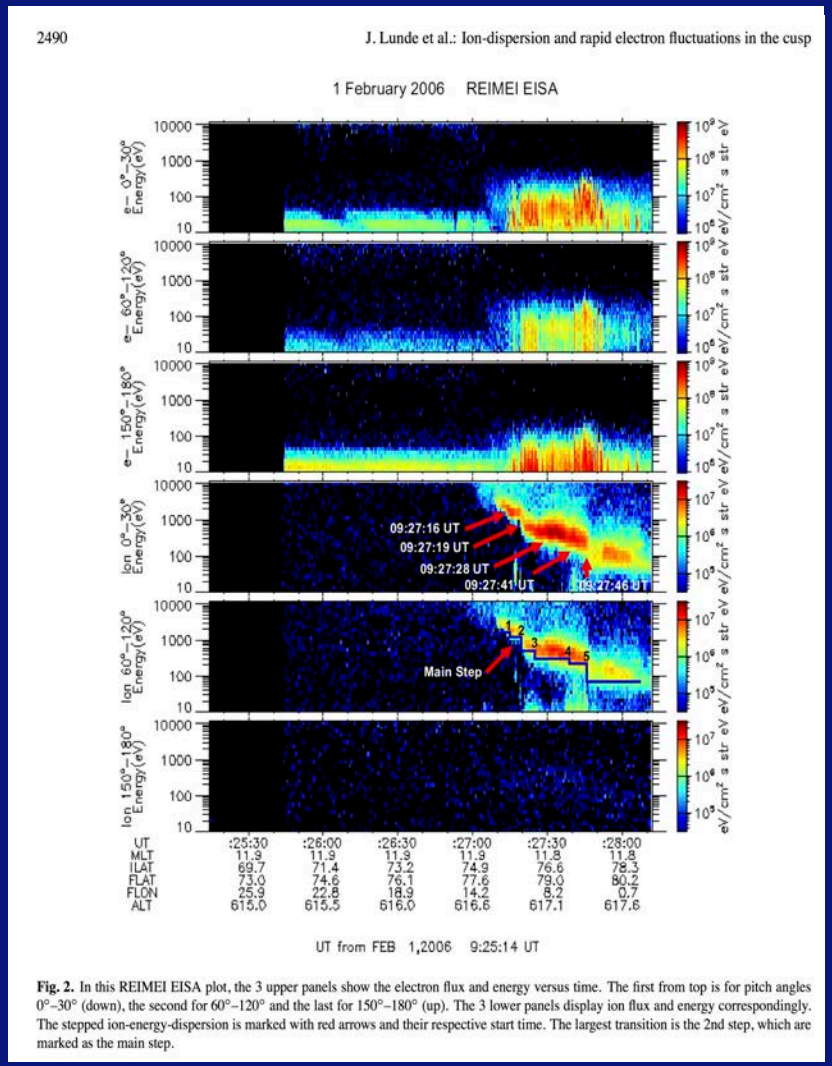

Fig. 2. In this REIMEI EISA plot, the 3 upper panels show the electron flux and energy versus time. The first from top is for pitch angles 0°–30° (down), the second for 60°–120° and the last for 150°–180° (up). The 3 lower panels display ion flux and energy correspondingly. The stepped ion-energy-dispersion is marked with red arrows and their respective start time. The largest transition is the 2nd step, which are marked as the main step.

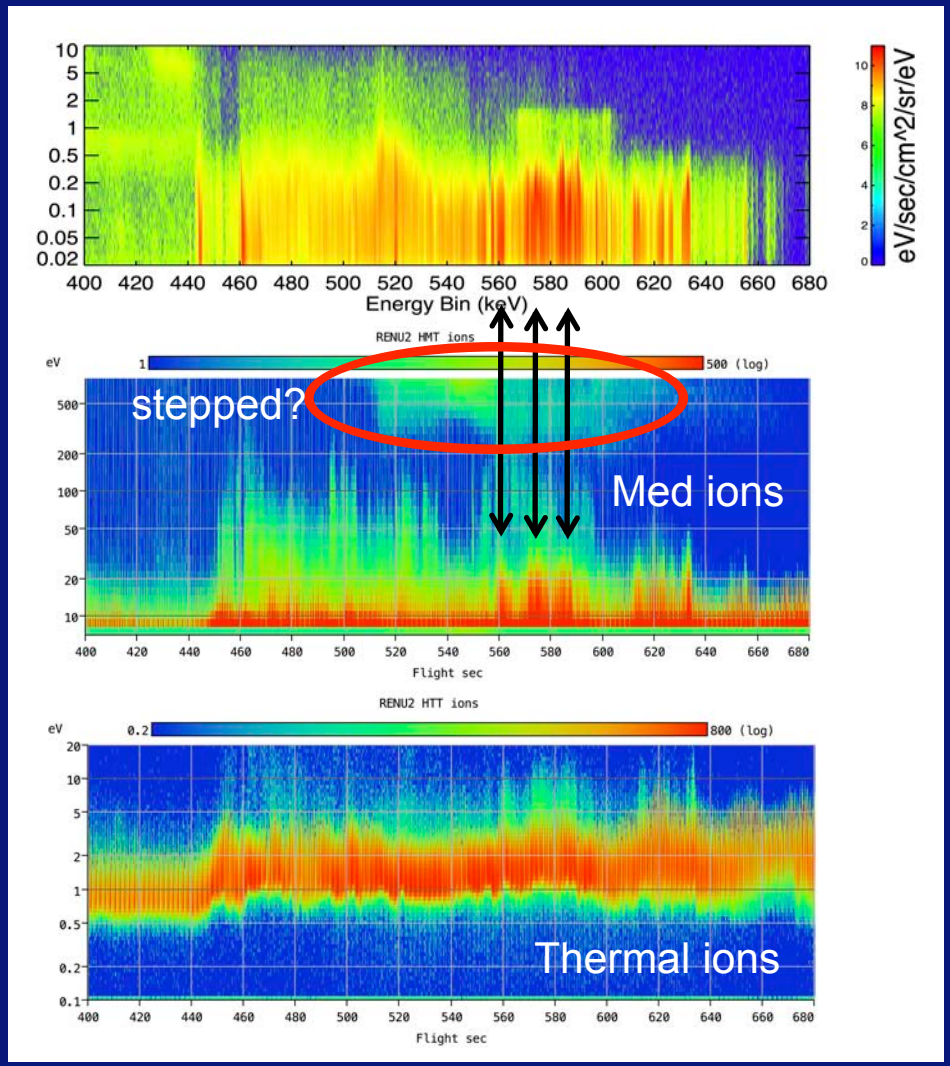

RENU2

Data – Aerospace Mag Ion Spec (J. Clemmons)

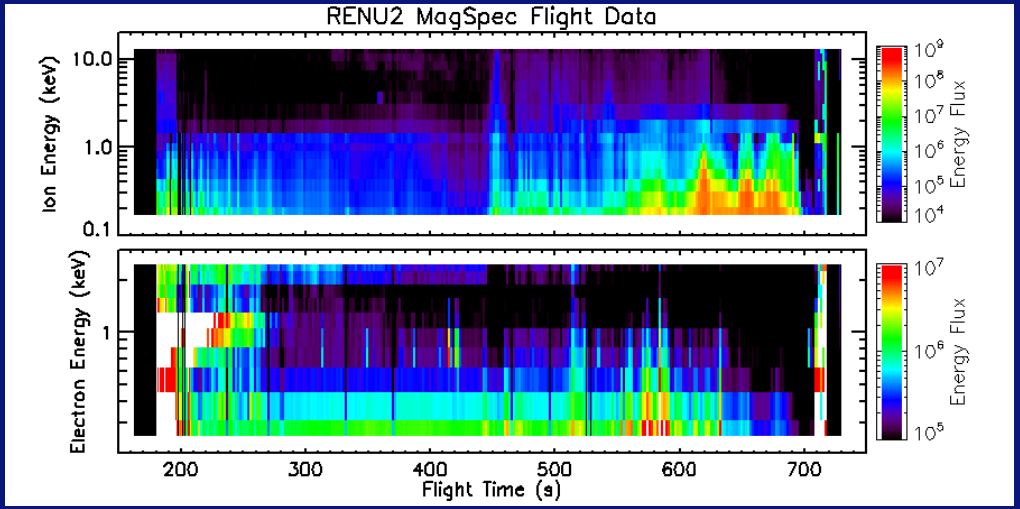

- Preliminary data , spin-averaged
  - ACS interference seen before 250 s
  - Some sensitivity adjustments still needed
- Clear boundary between “non-cusp” and “cusp” at 450 sCusp
  - Bursty ions seen across spectrum – common in cusp
  - Significant fluxes seen in 200 eV – 1 keV range (trapped TAI?)
  - Higher intensity, bursty lower energy electrons seen (instrument does not measure low enough to see “main” cusp electrons)

RENU2

Data – electric fields (Cornell, D. Hysell)

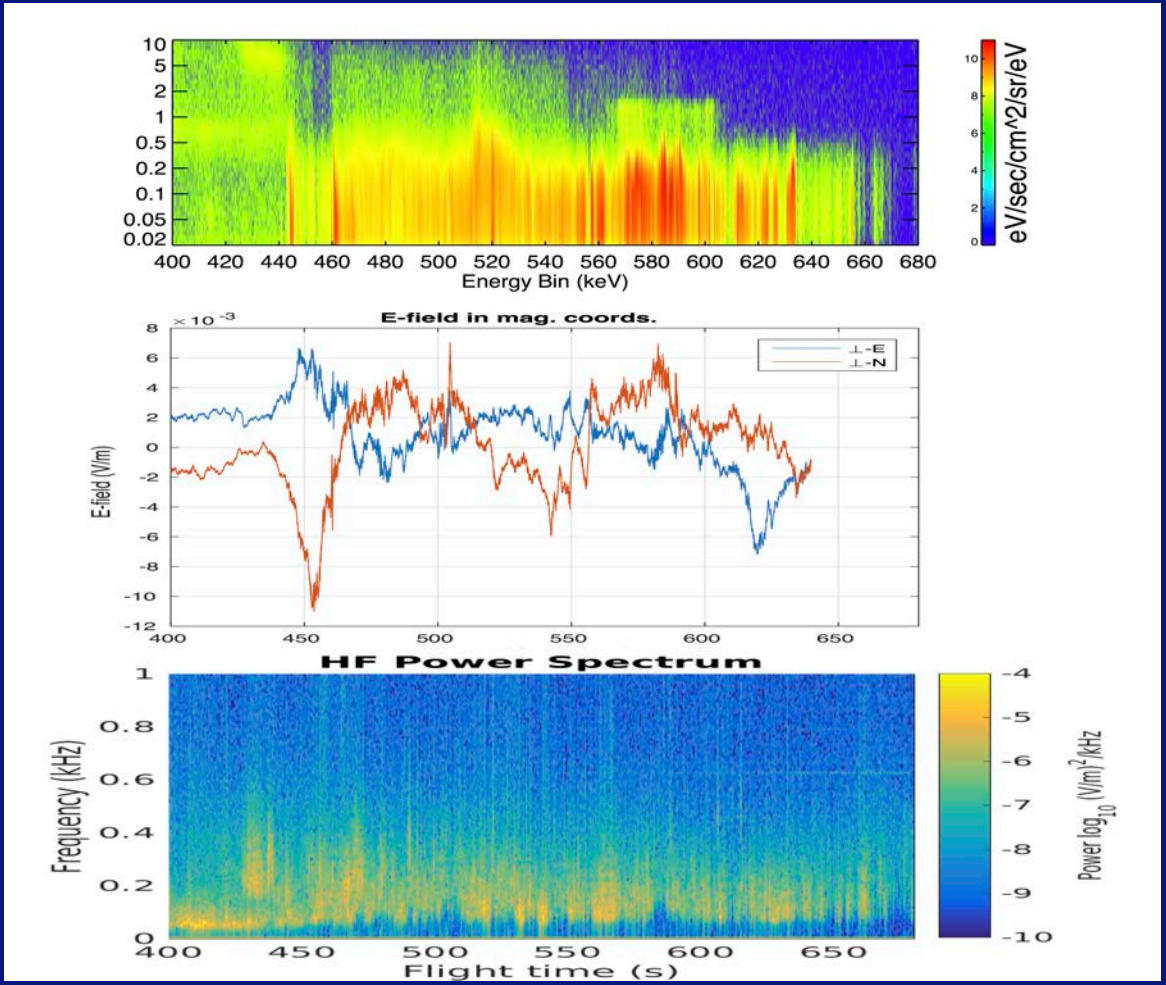

DC fields show:

- Counter-streaming flow NE-SW channels.

-The patterns flips polarity through the flight.

- Magnitudes of ~100-200 m/s.

RENU2 – Sunlit aurora

Data – Aerospace Phometers (J. Hecht)

Onboard observations of “sunlit aurora”, which are N2+ ions that have drifted upward. Have been observed up to 1000 km altitude.

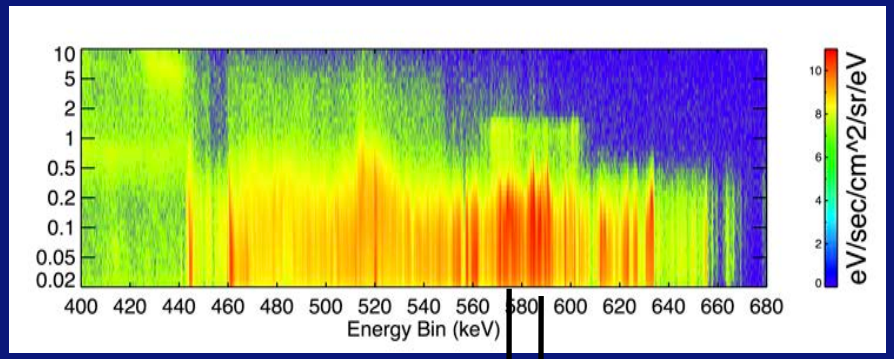

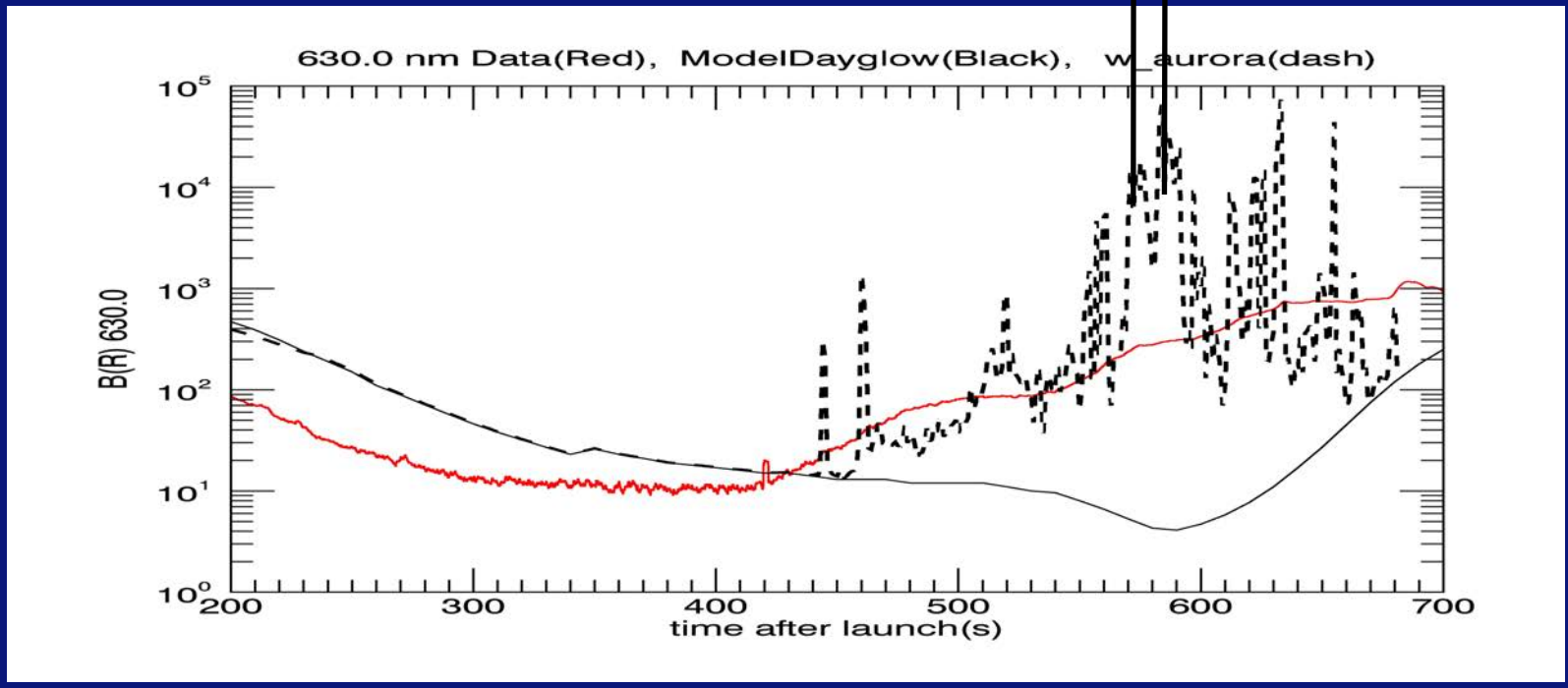

RENU2

About sunlit aurora

• Discovered by Carl Stormer, 1955, using ground data. Noted blue aurora extending up to 1000 km altitude; later determined to be UV-driven N2+ ions.

Stormer, C., 1955. The Polar Aurora. Clarendon Press, Oxford

• Interesting report in using the Solar Mass Ejection Imager (SMEI) on a USAF sun-synchronous satellite (840 km altitude) showing auroral filaments reaching 2000 km at high latitudes, conclude it is sunlit aurora.

Mizuno, D. R., et al. (2005), Very high altitude aurora observations with the Solar Mass Ejection Imager, J. Geophys. Res., 110, A07230, doi:10.1029/2004JA010689.

• From Ballistic Missile Defense Organization's (BMDO) Midcourse Space Experiment(MSX), report of 2.5 kR, implied number density of 10^3 ions/cm^3 at 900 km altitude.

Romick, G. J., J-H. Yee, M. F. Morgan, D. Morrison, L. J. Paxton and C-I. Meng, Polar Cap Optical Observationsof Topside(> 900 km) Molecular Nitrogen Ions , GRL 26, 1003-1006, April, 1999.

• Contribute 10% of number flux, seen rarely by Akebono, an alttiude of 5000 km.

Yau, A. W., B. A. Whalen, C. Goodenough, E. Sagawa, and T. Mukai (1993), EXOS D (Akebono) observations of molecular NO+ and N+2 upflowing ions in the high-altitude auroral ionosphere, J. Geophys. Res., 98, 11,205.

RENU2 – Neutrals

Data – Aerospace IG (J. Clemmons)

IG: Response in axial sensors normalized to MSIS

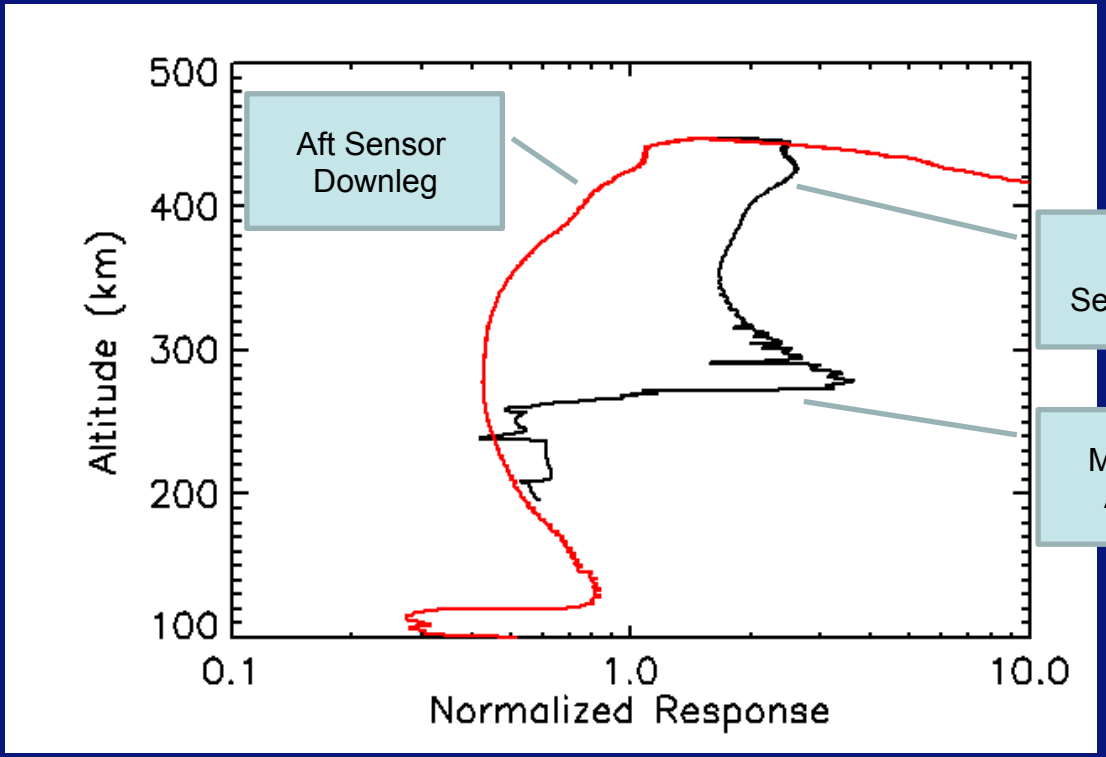

- Data from axial sensors normalized to MSIS predictions
- Upleg density apparently significantly enhanced over MSIS
- Downleg density apparently significantly depleted relative to MSIS
- Needs more work!

RENU2 – Neutrals

Data – UV PMT (UNH)

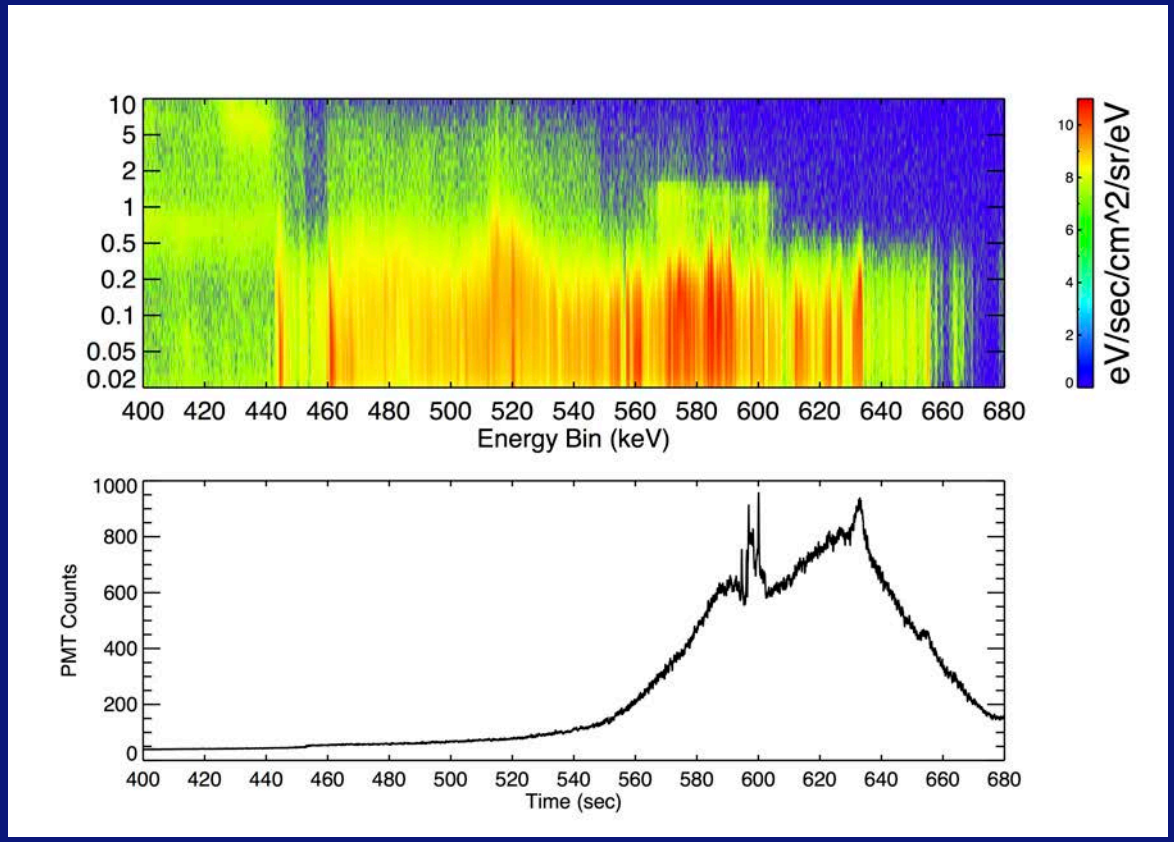

The UV PMT measures both 130.4 nm and 135.6 nm emissions, which are associated with atomic neutral oxygen.

The 135.6 nm emissions are produced by electron precipitation and perhaps provides the structure in the PMT signature.

The 130.4 nm line can be driven by either electron precipitation or by UV photoemissions. The lack of structure in the broad, featureless “bump” appear to be due to the photoemissions of background atomic oxygen.

RENU2

Data – DMSP UV observations

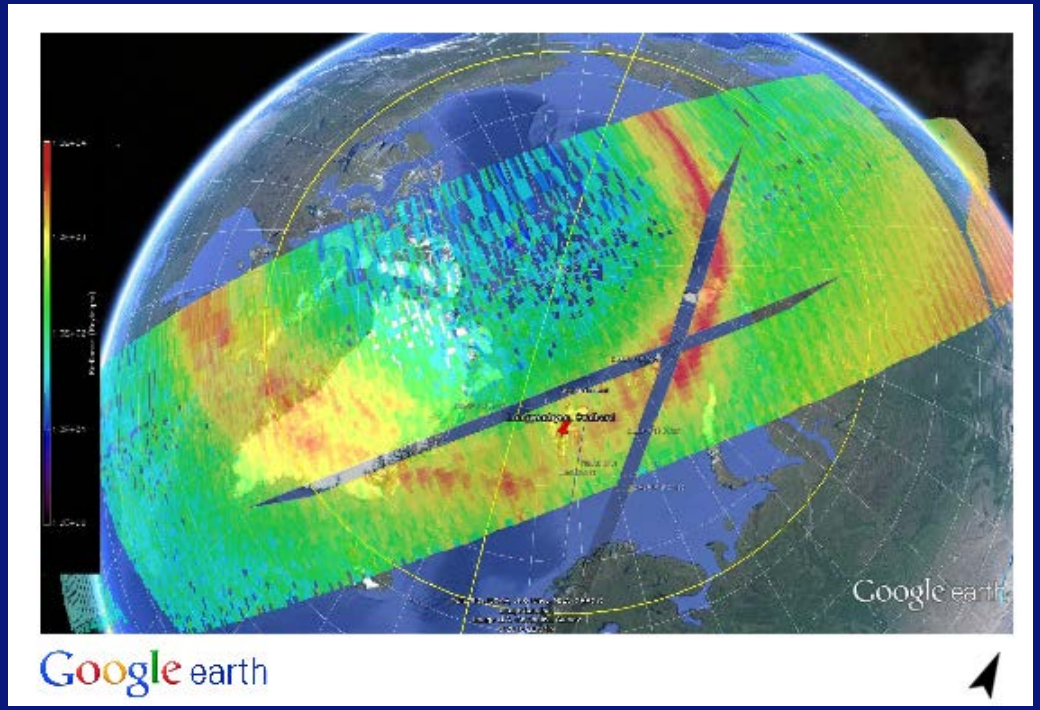

DMSP observations of a UV “pushbroom” scanner at 130.4 nm. DMSP passed over Svalbard ~10 minutes before RENU2 reached apogee. The arc appeared to intensify significantly during this time. These emissions on DMSP are mapped to 100 km altitude; RENU2 observations were from 350 to 200 km. Needs more work....

RENU2

Modeling efforts – A. Otto (UAF) and B. Sadler (UNH)

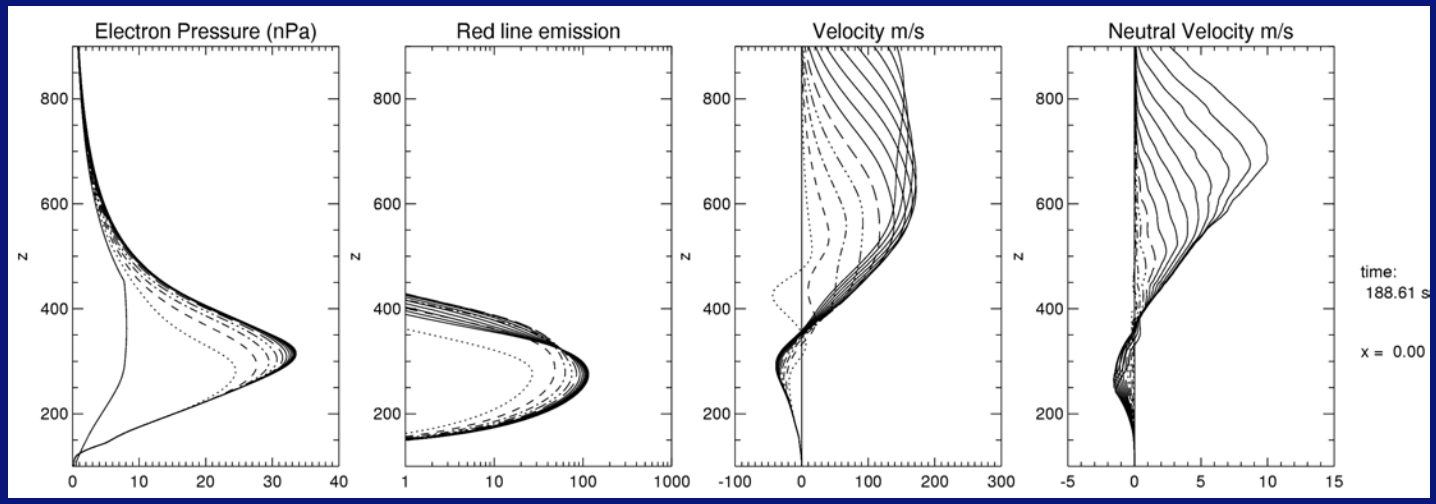

From A. Otto, from a 3-minute simulation of soft electron precipitation, with lines in each panel representing 15 second time-steps.

- 2-D calculation of ionosphere-magnetosphere interactions from 100 km to 1100 km with a gravitationally bound neutral atmosphere of N_2, O_2 and O.
- Atmosphere is based on an MSIS profile with a temperature of 1300 K in the F region and a fixed density at 100 km altitude.
- Input of 400 eV electrons, the model reveals an increase in temperature and density at about 320 km
- Maximum upward *ion* velocities reach about 200 m/s.

RENU2

Modeling efforts – A. Otto (UAF) and B. Sadler (UNH)

Temporal effects

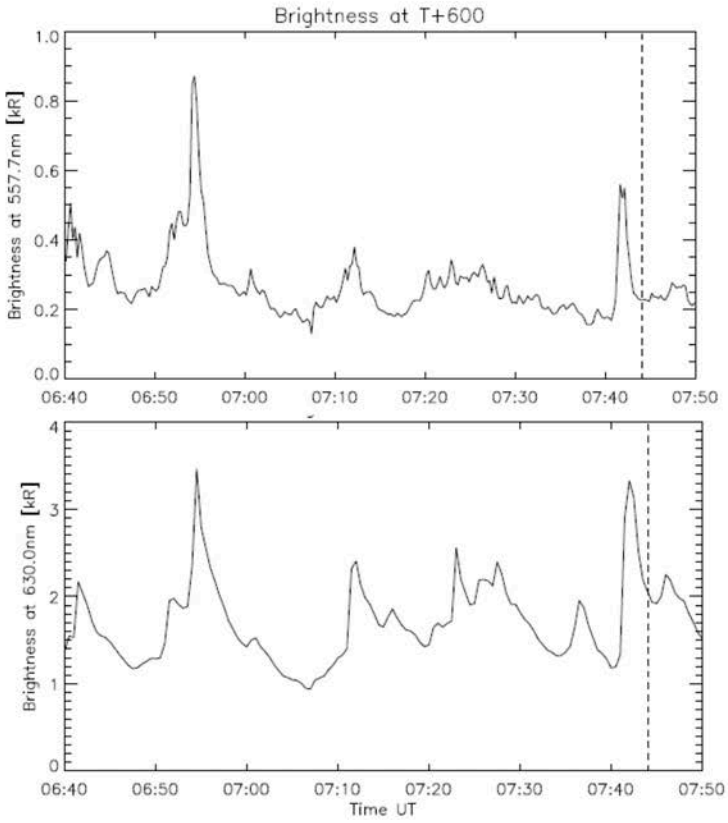

Brightness History
At footprint
Previous Hour

557.7 nm

630.0 nm

June 2, 2016

RENU2

Modeling efforts – A. Otto (UAF) and B. Sadler (UNH)
Temporal effects

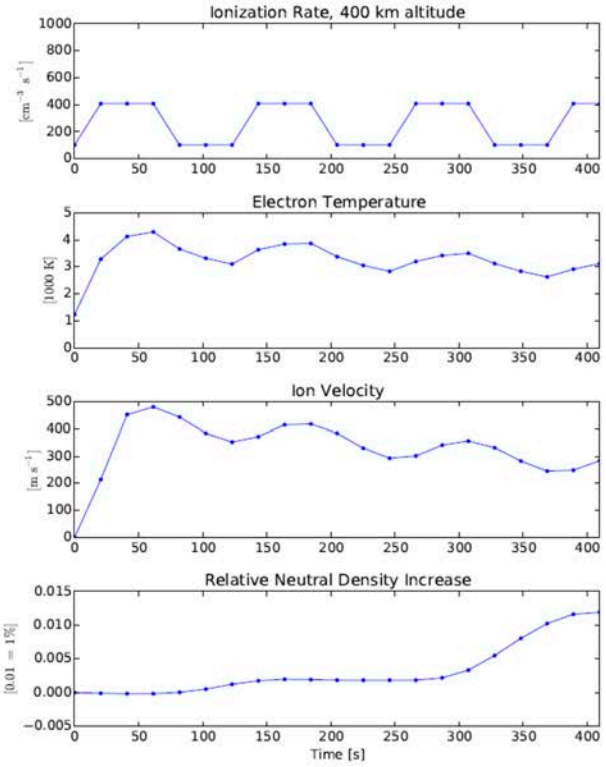

Model Results:

- Aurora pulsed on/of
- 150 eV electron energy
- 1 mW/m^2 background
- 4 mW/m^2 Aurora “on”

- 400s simulation
- On/off pulses at 66s

- Upward ion velocity remains high
- Neutral density increase w/ Aurora “off”

Aurora and ionosphere/thermosphere coupling

1. Energy is deposited via auroral precipitation in many different types of aurora and span a wide range of electron energies.

2. Coupling to the ionosphere and thermosphere is very common

3. Thermospheric effects include (at least) infrasonic signatures, gravity wave perturbations and “vertical winds” (or “neutral upwelling”, etc).

4. The relative contributions of energy from precipitating electrons versus Joule heating is an open question.